Extended SAID partial-wave analysis of pion photoproduction

William J. Briscoe,[1] Axel Schmidt,[1] Igor Strakovsky ⊙,[1,*] and Ron L. Workman[1]
(SAID Group)

Alfred Švarc[2,3]

[1]*Institute for Nuclear Studies, Department of Physics, The George Washington University, Washington, DC 20052, USA*
[2]*Rudjer Bošković Institute, 10000 Zagreb, Croatia*
[3]*Tesla Biotech d.o.o., 7 Mandlova, 10000 Zagreb, Croatia*

A unified Chew-Mandelstam description of single-pion photoproduction data, together with pion- and η-hadroproduction data, has been extended to include measurements carried out over the last decade. We consider photodecay amplitudes evaluated at the pole with particular emphasis on $n\gamma$ couplings and the influence of weighting on our fits. Both energy-dependent and single-energy analysis (energy-binned data) are considered.

I. INTRODUCTION

Our knowledge of the baryon spectrum, as determined from analyses of experimental data, has advanced rapidly [1] over the past decade. The progress has been most significant for nonstrange baryons, due largely to the wealth of new and more precise measurements made at electron accelerators worldwide. The majority of these new measurements have been performed at Jefferson Lab, USA (using the CLAS and Hall A detectors), with the MAMI accelerator in Mainz, Germany (the Crystal Ball/TAPS detector being particularly well suited for the measurement of neutral final states), and with the Crystal Barrel detector at ELSA in Bonn, Germany. While most of the early progress [2–5] in baryon spectroscopy was based on the analysis of meson-nucleon scattering data, particularly pion-nucleon scattering ($\pi N \to \pi N$, $\pi N \to \pi \pi N$), photon-nucleon interactions offer the possibility of detecting unstable intermediate states with small branchings to the πN channel. Many groups have performed either single-channel or multichannel analyses of these photon-induced reactions. In the more recent single-channel analyses, fits have typically used isobar models [6,7] with unitarity constraints at the lower energies, K-matrix-based formalisms, having built-in cuts associated with inelastic channels [8], and dispersion-relation constraints [7,9]. Multichannel fits have analyzed data (or, in some cases, amplitudes) from hadronic scattering experiments together with the photon-induced channels. These approaches have utilized unitarity more directly. Among others, analyses

have been carried out by MAID [6], the Bonn-Gatchina [10], ANL-Osaka [11], Kent State [12], and JPAC [13] groups, SAID [8] (Scattering Analysis Interactive Database), and Jülich-Bonn [14]. Here, we should also briefly mention the possibility of extracting reaction amplitudes directly from scattering data with minimal model input. Examples of this approach are described in the analyses of kaon photoproduction data by the Jefferson Lab [15] and Bonn-Gatchina [16] groups. The measurements required for an amplitude extraction with minimal model bias differ depending on whether the goal is to obtain helicity amplitudes (the usual *complete experiment* case [17]) or partial-wave amplitudes [18]. A number of recent studies have shown the limits to model independence [19] and the convergence [20] of independent fits with the availability of more observables measured with high precision. The above studies have also recently been extended to pseudo-scalar-meson electroproduction [21].

An objective of this program is the determination of all relevant characteristics of these resonances, i.e., pole positions, widths, principal decay channels, and branching ratios. In order to compare directly with quantum chromodynamics (QCD)-inspired models and lattice QCD predictions, there has also been a considerable effort to find "hidden" or "missing" resonances [22], predicted by quark models [23] and LQCD [24] but not yet confirmed. Actually, the Particle Data Group (PDG) [1] reports a third of predicted states by constituent quark models and LQCD.

Knowledge of the N and Δ resonance photodecay amplitudes has largely been restricted to the charged states. Apart from lower-energy inverse reaction $\pi^- p \to \gamma n$ measurements, the extraction of the two-body $\gamma n \to \pi^- p$ and $\gamma n \to \pi^0 n$ observables requires the use of a model-dependent nuclear correction, which mainly comes from final state interaction (FSI) effects within the target deuteron [25–27]. As a result, the observables for proton-target experiments are most thoroughly explored and, among neutron-target (deuteron) measurements, the $\pi^0 n$ charge channel is least explored.

*Corresponding author: igor@gwu.edu

TABLE I. Published data for $\gamma N \to \pi N$ reactions since 2012 as given in the SAID database [32]: first column is the reaction, second column is the observable, third column is the number of energy bins, fourth column is the number of data points.

Reaction	Observable	Nexp	Ndata	E_γ(min) (MeV)	E_γ(max) (MeV)	θ(min) (deg)	θ(max) (deg)	Laboratory/Collaboration	Ref.
$\gamma p \to \pi^0 p$	$d\sigma/d\Omega$	30	600	147	218	18	162	MAMI/A2	[39]
		269	7978	218	1573	15	165	MAMI/A2	[40]
		41	560	862	2475	15	165	CBELSA/CBELSA/TAPS	[41]
		80	2030	1275	5425	27	140	JLab/CLAS	[42]
		22	350	1325	2375	47	162	SPring-8/LEPS2&BGOegg	[43]
	Σ	26	220	147	206	25	155	MAMI/A2	[39]
		78	1403	319	649	31	158	MAMI/A2	[44]
		39	700	1102	1862	32	148	JLab/CLAS	[34]
		16	252	1325	2350	57	162	SPring-8/LEPS2&BGOegg	[43]
	$\mathbb{P}$	8	152	683	917	51	163	CBELSA/CBELSA/TAPS	[45]
		11	11	1845	5631	79	143	JLab/GEp-III & GEp2gamma	[46]
	$\mathbb{T}$	245	4343	151	419	5	175	MAMI/A2	[47]
		34	397	440	1430	30	162	MAMI/A2	[48]
		29	601	683	2805	29	163	CBELSA/CBELSA/TAPS	[45]
	$\mathbb{E}$	33	456	615	2250	22	158	CBELSA/CBELSA/TAPS	[49]
	$\mathbb{G}$	22	197	632	2187	37	144	JLab/CLAS	[50]
		19	318	633	1300	23	156	CBELSA/CBELSA/TAPS	[51]
	$\mathbb{F}$	34	397	440	1430	30	162	MAMI/A2	[48]
	$\mathbb{H}$	8	154	683	917	51	163	CBELSA/CBELSA/TAPS	[45]
	$\mathbb{C}_{x'}$	45	45	462	1337	75	140	MAMI/A2	[52]
		13	13	1845	5643	82	143	JLab/GEp-III & GEp2gamma	[46]
	$\mathbb{C}_{z'}$	13	13	1845	5643	80	143	JLab/GEp-III & GEp2gamma	[46]
$\gamma p \to \pi^+ n$	Σ	39	386	1102	1862	32	148	JLab/CLAS	[34]
	$\mathbb{E}$	35	900	363	2181	20	146	JLab/CLAS	[53]
	$\mathbb{G}$	22	216	632	2229	29	142	MAMI/A2	[50]
$\gamma n \to \pi^- p$	σ_{tot}	6	6	150	162			MAX-lab/PIONS@MAX-lab	[54]
	$d\sigma/d\Omega$	14	104	301	455	58	133	MAMI/A2	[55]
		156	8428	445	2510	26	128	JLab/CLAS	[35]
		68	816	1050	3500	32	157	JLab/CLAS	[33]
	Σ	93	1293	947	2498	24	145	JLab/CLAS	[56]
	$\mathbb{E}$	21	266	727	2345	26	154	JLab/CLAS	[36]
$\gamma n \to \pi^0 n$	$d\sigma/d\Omega$	27	492	290	813	32	139	MAMI/A2	[37]
		49	931	446	1427	32	162	MAMI/A2	[57]
	Σ	12	189	390	610	49	148	MAMI/A2	[29]
	$\mathbb{E}$	17	151	446	1427	46	154	MAMI/A2	[58]

This problem is less severe if isospin relations are used to express the four charge-channel amplitudes in terms of three isospin amplitudes [28]. Then, in principle, the $\pi^0 n$ production channel can be predicted in terms of the $\pi^0 p$, $\pi^+ n$ and, $\pi^- p$ production channel amplitudes. This approach has been tested [29] with the improved availability of $\pi^0 n$ data; we will consider this again in the fits to data that follow.

The George Washington University (GW) SAID pion photoproduction analyses have been updated periodically since 1990 [30,31], with more frequent updates published through our GW website [32]. Often, we present our results with CLAS and A2 Collaborations including determination of the resonance parameters (see, for instance, Refs. [33–37]) while our full analysis was reported ten years ago [8,38]. The present work updates our SAID partial-wave analysis (PWA) results and reports a new determination of photode-

cay amplitudes and pole positions in the complex energy plane.

High activity of worldwide electromagnetic facilities (JLab, MAMI, CBELSA, MAX-lab, SPring-8, and ELPH) increased the body of the SAID database by a significant amount (see Table I). 60% of these are $\gamma p \to \pi^0 p$ data. A review of the last two decades of using photon beams to measure the production of mesons, and in particular the information that can be obtained on the spectrum of light, non-strange baryons is given in Ref. [59]. A wealth of $\gamma N \to \pi N$ data, for single- and double-polarization observables, have been anticipated over the past ten years. These data are pivotal in determining the underlying amplitudes in nearly complete experiments, and in discerning between various microscopic models of multichannel reaction theory.

The amplitudes from these analyses can be utilized, in particular, in evaluating contributions to the Gerasimov-Drell-

TABLE II. Comparison of χ^2 per datum values for all charged and neutral channels covering fit energy range. The previous SAID fit, CM12, was published in Ref. [8] (and is valid up to $E_\gamma = 2700$ MeV). CM12 is compared to both the current database and data before 2012. All data are available in the SAID database (DB) [32]. For the SM44 fit, $\pi^0 n$ data were weighted by an arbitrary factor of 4. For the WM22 fit, all data with large χ^2/data for the SM22 solution (SM22 is our main result, data are listed in Table III) were weighted by an arbitrary factor of 4. The NM22 solution represents a fit without the inclusion of $\pi^0 n$ data. The previous MAID2007 solution is valid up to $E_\gamma = 1680$ MeV ($W = 2$ GeV) [6].

Solution	Observable	$\chi^2/(\pi^0 p$ data)	$\chi^2/(\pi^+ n$ data)	$\chi^2/(\pi^- p$ data)	$\chi^2/(\pi^0 n$ data)
SM22	Total	30399/15901 = 1.92	13945/6194 = 2.25	12267/6662 = 1.84	4190/1205 = 3.48
	UnPol	9842/5730 = 1.72	4984/2603 = 1.91	7497/4706 = 1.59	1995/649 = 3.07
	SinglePol	16036/8249 = 1.94	6078/2483 = 2.45	4014/1684 = 2.38	1258/405 = 3.11
	DoublePol	4521/1922 = 2.35	2883/1108 = 2.60	765/275 = 2.78	937/151 = 6.21
SM44	Total	30870/15901 = 1.94	14293/6194 = 2.31	12358/6662 = 1.86	3361/1205 = 2.79
	UnPol	9880/5730 = 1.72	5154/2603 = 1.98	7832/4706 = 1.66	1648/649 = 2.54
	SinglePol	16405/8249 = 1.99	6229/2483 = 2.51	3830/1684 = 2.27	823/405 = 2.03
	DoublePol	4585/1922 = 2.39	2910/1108 = 2.63	696/275 = 2.53	890/151 = 5.89
NM22	Total	29998/15901 = 1.89	13592/6194 = 2.19	11992/6662 = 1.80	8531/1205 = 7.08
	UnPol	9887/5730 = 1.73	4757/2603 = 1.83	7262/4706 = 1.54	2322/649 = 3.58
	SinglePol	15662/8240 = 1.90	5915/2483 = 2.38	3746/1684 = 2.22	4570/405 = 11.28
	DoublePol	4449/1922 = 2.31	2920/1108 = 2.64	984/275 = 3.58	1639/151 = 10.85
WM22	Total	31315/15901 = 1.97	14038/6194 = 2.27	12819/6662 = 1.92	3853/1205 = 3.20
	UnPol	9816/5730 = 1.71	4659/2603 = 1.79	7735/4706 = 1.64	2113/649 = 3.26
	SinglePol	16922/8249 = 2.05	6537/2483 = 2.63	4258/1684 = 2.53	885/405 = 2.19
	DoublePol	4577/1922 = 2.38	2.842/1108 = 2.57	826/275 = 3.00	855/151 = 5.66
CM12 (current DB)	Total	78254/15901 = 4.92	27933/6194 = 4.51	222454/6662 = 33.39	7024/1205 = 5.89
	UnPol	18074/5730 = 3.15	4565/2603 = 1.75	65514/4706 = 13.92	4063/649 = 6.26
	SinglePol	50016/8249 = 6.06	12221/2483 = 4.92	154303/1684 = 91.62	976/405 = 2.41
	DoublePol	10164/1922 = 5.26	11147/1108 = 10.06	2637/275 = 9.59	1985/151 = 13.15
CM12 (old DB)	Total	10544/4507 = 2.34	10444/4916 = 2.12	2486/1509 = 1.65	987/373 = 2.65
	UnPol	2682/1094 = 2.45	4247/2459 = 1.73	1769/1118 = 1.58	475/157 = 3.03
	SinglePol	5846/2723 = 2.15	3312/1523 = 2.18	564/304 = 1.86	512/216 = 2.37
	DoublePol	2016/690 = 2.92	2885/934 = 3.09	153/87 = 0.82	
MAID2007 (current DB)	Total	170832/14454 = 11.82	128063/5396 = 23.73	102968/5520 = 18.65	29390/1205 = 24.39
	UnPol	74153/5188 = 14.29	24533/2210 = 11.10	40840/4166 = 9.80	2812/649 = 4.33
	SinglePol	84286/7578 = 11.12	96337/2168 = 44.44	59097/1182 = 50.00	22087/405 = 54.54
	DoublePol	12393/1688 = 7.34	7193/1018 = 7.07	3031/172 = 17.62	4494/151 = 29.76

Hearn (GDH) sum rule and related integrals, as was reported recently [60].

In the following section (Sec. II), we summarize changes to the SAID database since 2012. The changes reflected in our multipoles are displayed in Sec. III. A comparison of past and recent photodecay amplitudes, for resonances giving a significant contribution to pion photoproduction, is made in Sec. IV. Finally, in Sec. V, we summarize our results and comment on possible changes due to further measurements and changes in our parametrization form.

II. EXTENDED SAID DATABASE

At present, the SAID database [32] has 35 898 $\gamma p \to \pi^0 p$, 12 494 $\gamma p \to \pi^+ n$, 13 473 $\gamma n \to \pi^- p$, and 2515 $\gamma n \to \pi^0 n$ data below $E_\gamma = 2700$ MeV.

Table I accumulates 21 190 $\gamma p \to \pi^0 p$, 1502 $\gamma p \to \pi^+ n$, 10 923 $\gamma n \to \pi^- p$, and 1763 $\gamma n \to \pi^0 n$ data published since 2012 [32]. New measurements mostly cover the $\pi^0 p$ sector. Then there are a lot of single (Σ, $\mathbb{P}$, and $\mathbb{T}$), and double ($\mathbb{E}$, $\mathbb{G}$, $\mathbb{F}$, and $\mathbb{H}$) polarized data which came recently. It

is an essential input for the amplitude reconstruction of the pion photoproduction and determination photocouplings. One can see that the "neutron" database grows rapidly which is important for the determination of the neutral photocouplings.

A full χ^2/data contribution for each pion photoproduction reaction vs different PWAs reports in Table II. It presents a partial χ^2/data contribution of data from Table III vs different PWAs.

III. SAID MULTIPOLE AMPLITUDES

The SAID parametrization of the transition amplitude $T_{\alpha\beta}$ used in the hadronic fits to the πN scattering data is given as

$$T_{\alpha\beta} = \sum_\sigma [1 - \overline{K} C]_{\alpha\sigma}^{-1} \overline{K_{\sigma\beta}}, \qquad (1)$$

where α, β, and σ are channel indices for the πN, $\pi \Delta$, ρN, and ηN channels. Here, $\overline{K_{\sigma\beta}}$ are the Chew-Mandelstam K matrices, which are parametrized as polynomials in the scattering energy. C_α is the Chew-Mandelstam function, an element of a diagonal matrix C in channel space, which is

TABLE III. List of data with large χ^2/data for the SM22 and associated fits. Notation for solutions is given in the caption of Table II.

Reaction	Obs	E_γ (MeV)	Data	MAID2007 χ^2/data	CM12 χ^2/data	SM22 χ^2/data	SM44 χ^2/data	WM22 χ^2/data	NM22 χ^2/data	Ref.
$\gamma p \to \pi^0 p$	$d\sigma/d\Omega$	675–2875	620	40.56	2.38	3.28	3.09	2.18	3.34	[61]
	$\mathbb{P}$	1845–2776	3		242.	107.	83.1	26.13	89.01	[46]
		773–2472	29	8.47	5.45	12.83	12.93	8.69	13.10	[62]
	$\mathbb{G}$	632–2187	197	11.45	46.34	4.23	4.43	4.02	3.87	[50]
	$\mathbb{C}_{x'}$	1845–2776	3		985.	8.75	5.18	9.39	7.53	[46]
		773–2472	28	28.25	9.96	7.64	7.82	4.89	8.39	[62]
	$\mathbb{C}_{z'}$	1845–	3		1370.	8.68	14.40	2.46	7.87	[46]
		773–2472	25	35.44	12.80	12.00	8.44	9.16	13.28	[62]
$\gamma p \to \pi^+ n$	$d\sigma/d\Omega$	725–2875	618	65.71	2.08	2.75	2.83	1.82	2.44	[63]
	$\mathbb{G}$	632–2229	216	21.09	25.33	4.42	4.66	3.57	4.49	[50]
$\gamma n \to \pi^0 n$	Σ	703–1475	216	100.1	2.37	4.72	2.81	2.93	19.26	[64]
	$\mathbb{E}$	446–1427	151	29.75	13.14	6.21	5.89	5.66	10.85	[58]

expressed as a dispersion integral with an imaginary part equal to the two-body phase space [65].

In Ref. [8], it was shown that this form could be extended to $T_{\alpha\gamma}$ to include the electromagnetic channel as

$$T_{\alpha\gamma} = \sum_\sigma [1 - \overline{K}C]^{-1}_{\alpha\sigma}\overline{K_{\sigma\gamma}}\,. \qquad (2)$$

Here, the Chew-Mandelstam K-matrix elements associated with the hadronic channels are kept fixed from the previous SAID solution SP06 [3], and only the electromagnetic elements are varied. The resonance pole and cut structures are also fixed from hadronic scattering. This provides a minimal description of the photoproduction process, where only the N^* and Δ^* states present in the SAID πN scattering amplitudes are included in this multipole analysis.

For each angular distribution, a normalization constant (X) and its uncertainty (ϵ_X) were assigned. The quantity ϵ_X is generally associated with the normalization uncertainty (if known). The modified χ^2 function to be minimized is given by

$$\chi^2 = \sum_i \left(\frac{X\theta_i - \theta_i^{\exp}}{\epsilon_i}\right)^2 + \left(\frac{X - 1}{\epsilon_X}\right)^2, \qquad (3)$$

where the subscript i labels the data points within the distribution, $\theta_i^{\exp}$ is an individual measurement, θ_i is the corresponding calculated value, and ϵ_i represents the total angle-dependent uncertainty. The total χ^2 is then found by summing over all measurements. This re-normalization freedom is essential for obtaining the best SAID fit results. For other data analyzed in the fit, such as the total cross sections and excitation data, the statistical and systematic uncertainties were combined in quadrature and no renormalization was allowed.

In the previous fits to differential cross sections, the unrestricted best fit gave re-normalization constants X significantly different from unity. As can be seen from Eq. (3), if an angular distribution contains many measurements with small statistical uncertainties, a change in the renormalization may improve the fit with only a modest χ^2 penalty. Here, however, the weight of the second term in Eq. (3) has been adjusted by

the fit for each dataset to keep the re-normalization constants approximately within X of unity.

With the new quality datasets (Table I), a new SAID multipole analysis has been completed. This new global energy-dependent solution has been labeled as SM22. The overall fit quality of the present SM22 and previous SAID CM12 solutions are compared in Tables III and IV. There are many cases where the CM12 fit produces a χ^2 per datum, for new measurements, which is significantly than greater than unity. The new best fit, SM22, includes these new measurements, reducing the χ^2/data to more acceptable values.

Both energy-dependent (ED) and single-energy (SE) solutions were obtained from fits to the combined proton and neutron target database, extending from threshold to $E_\gamma = 2.7$ GeV for the ED fit and to $E_\gamma = 2.2$ GeV for SE fits.

Apart from the main ED result (SM22) several supplemental fits were done in order to gauge the importance of including $\pi^0 n$ data (which can, in principle, be at least qualitatively predicted from the remaining more fully populated charge channels). Here, fits were done with increased weight for the $\pi^0 n$ data and conversely the removal of all such data. In addition, a fit was done more heavily weighting all data poorly fitted by SM22. Figures 1 and 2 plot representative comparisons of SAID fits to data. In addition, older MAID and more recent Bonn-Gatchina results are plotted for comparison. Numerical comparisons of the various SAID fits are given in Tables II to IV.

Comparisons of the present SAID $I = 3/2$ and $I = 1/2$ multipoles amplitudes from threshold to $W = 2.5$ GeV ($E_\gamma = 2.7$ GeV) shown in Figs. 3–8. Also included, for comparison, are the BnGa and MAID multipoles.

Comparisons of the present $I = 3/2$ and $I = 1/2$ ED and SE multipole amplitudes from threshold to $W = 2.5$ GeV ($E_\gamma = 2.7$ GeV) shown on Figs. 9–14.

IV. RESONANCE COUPLINGS

Following the notation of Refs. [38,70], the (γ, π) T-matrix element for helicity h is given by

$$T_{\gamma,\pi}^h = \sqrt{2\,k\,q}\,\mathcal{A}_\alpha^h\,C\,, \qquad (4)$$

TABLE IV. Comparison χ^2/data for published data since 2012 as given in Table I and available in the SAID database [32]. Notation for solutions is given in the caption of Table II. Data, which are partially (completely) excluded in the SAID fits, denoted by [‡] ([†]).

Reaction	Obs	MAID2007 χ^2/data	CM12 χ^2/data	SM22 χ^2/data	SM44 χ^2/data	WM22 χ^2/data	NM22 χ^2/data	Ref.
$\gamma p \to \pi^0 p$	$d\sigma/d\Omega$	10.44	7.08	1.32	1.36	1.32	1.33	[39][‡]
		12.50	3.01	1.40	1.44	1.51	1.40	[40][‡]
		4.44	2.33	3.46	3.41	3.22	3.49	[41][†]
		18.28	2.34	2.69	2.50	2.37	2.77	[42][†]
		16.15	3.63	2.39	2.31	2.74	2.45	[43]
	Σ	41.69	0.99	1.40	1.39	1.33	1.39	[39]
		2.25	1.42	1.16	1.12	1.22	1.17	[44][‡]
		72.13	43.81	3.62	3.87	4.04	3.47	[34]
		4.93	11.21	1.95	1.96	2.46	1.81	[43]
	$\mathbb{P}$	2.13	1.50	1.04	1.09	1.17	1.05	[45]
			241.0	6.47	82.62	26.1	89.01	[46]
	$\mathbb{T}$	1.30	1.41	1.06	1.07	1.09	1.04	[47][‡]
		9.15	5.80	3.09	3.25	3.28	2.94	[48]
		12.25	4.14	2.17	2.24	2.43	2.05	[45]
	$\mathbb{E}$	15.14	4.22	2.11	2.20	2.62	2.03	[49]
	$\mathbb{G}$	11.45	6.38	4.23	4.43	4.02	4.20	[50]
		3.42	3.90	1.26	1.26	1.21	1.20	[51]
	$\mathbb{F}$	3.48	3.34	2.33	2.34	2.26	2.28	[48]
	$\mathbb{H}$	4.38	6.25	1.70	1.96	1.89	1.44	[45]
	$\mathbb{C}_{x'}$	2.07	2.36	1.71	1.71	1.76	1.73	[52]
			984.0	8.90	5.28	9.53	7.53	[46]
	$\mathbb{C}_{z'}$		1370.	8.74	14.49	2.48	7.87	[46]
$\gamma p \to \pi^+ n$	Σ	285.1	18.37	3.00	3.14	3.81	2.97	[34]
	$\mathbb{E}$	5.09	9.82	1.96	1.86	2.21	2.03	[53][‡]
	$\mathbb{G}$	21.09	25.33	4.42	6.64	3.57	4.49	[50]
$\gamma n \to \pi^- p$	σ_{tot}	0.33	0.05	0.06	0.20	0.10	0.90	[54]
	$d\sigma/d\Omega$	5.99	4.61	3.27	3.96	2.78	3.22	[55]
		14.88	20.39	1.28	1.30	1.33	1.25	[35][‡]
		30.39	76.83	3.97	3.97	3.77	4.17	[33][†]
	Σ	7.21	118.8	2.38	2.27	2.57	2.24	[56]
	$\mathbb{E}$	18.25	17.43	2.84	2.62	3.11	3.68	[36]
$\gamma n \to \pi^0 n$	$d\sigma/d\Omega$	3.77	7.29	2.88	2.43	3.14	3.89	[37]
		20.32	18.72	11.22	9.52	9.97	15.73	[57][†]
	Σ	2.44	2.46	1.25	1.15	1.33	2.17	[29]
	$\mathbb{E}$	29.75	13.11	6.21	5.89	5.66	10.85	[58]

where α denotes the partial wave and k, q are the center-of-mass (c.m.) momenta of the photon and the pion. The factor C is $\sqrt{2/3}$ for isospin 3/2 and $-\sqrt{3}$ for isospin 1/2. The helicity multipoles $\mathcal{A}_\alpha^h$ are given in terms of electric and magnetic multipoles

$$\mathcal{A}_{\ell+}^{1/2} = -\frac{1}{2}[(\ell+2)E_{\ell+} + \ell M_{\ell+}], \qquad (5)$$

$$\mathcal{A}_{\ell+}^{3/2} = \frac{1}{2}\sqrt{\ell(\ell+2)}[E_{\ell+} - M_{\ell+}], \qquad (6)$$

$$\mathcal{A}_{(\ell+1)-}^{1/2} = -\frac{1}{2}[\ell E_{(\ell+1)-} - (\ell+2)M_{(\ell+1)-}], \qquad (7)$$

$$\mathcal{A}_{(\ell+1)-}^{3/2} = -\frac{1}{2}\sqrt{\ell(\ell+2)}[E_{(\ell+1)-} + M_{(\ell+1)-}] \qquad (8)$$

with $J = \ell + 1/2$ for "+" multipoles and $J = (\ell+1) - 1/2$ for "−" multipoles, all having the same total spin J.

In Tables V–XIV, we list the pole positions together with the photodecay amplitudes

$$A_h = C\sqrt{\frac{q_p}{k_p}\frac{2\pi(2J+1)W_p}{m_N \text{Res}_{\pi N}}}\,\text{Res}\,\mathcal{A}_\alpha^h\,, \qquad (9)$$

where the subscript p denotes quantities evaluated at the pole position and m_N is the nucleon mass. In Ref. [38], the elastic residues, $Res_{\pi N}$, and the pole positions, $W_p = M_p - i\Gamma_p/2$, were taken from the GWU SAID PWA, SP06 [3] and each multipole was fitted separately, using the Laurent plus Pietarinen (L + P) method [38], to determine the corresponding residues.

Here, we have made a coupled multipole fit of all partial-wave amplitudes associated with particular resonances, including the pion-nucleon elastic scattering amplitudes. Thus, for example, the L + P fit of Ref. [38] for the $E_{2-}^{1/2}$ multipole has been expanded to a simultaneous fit of the D_{13} elastic
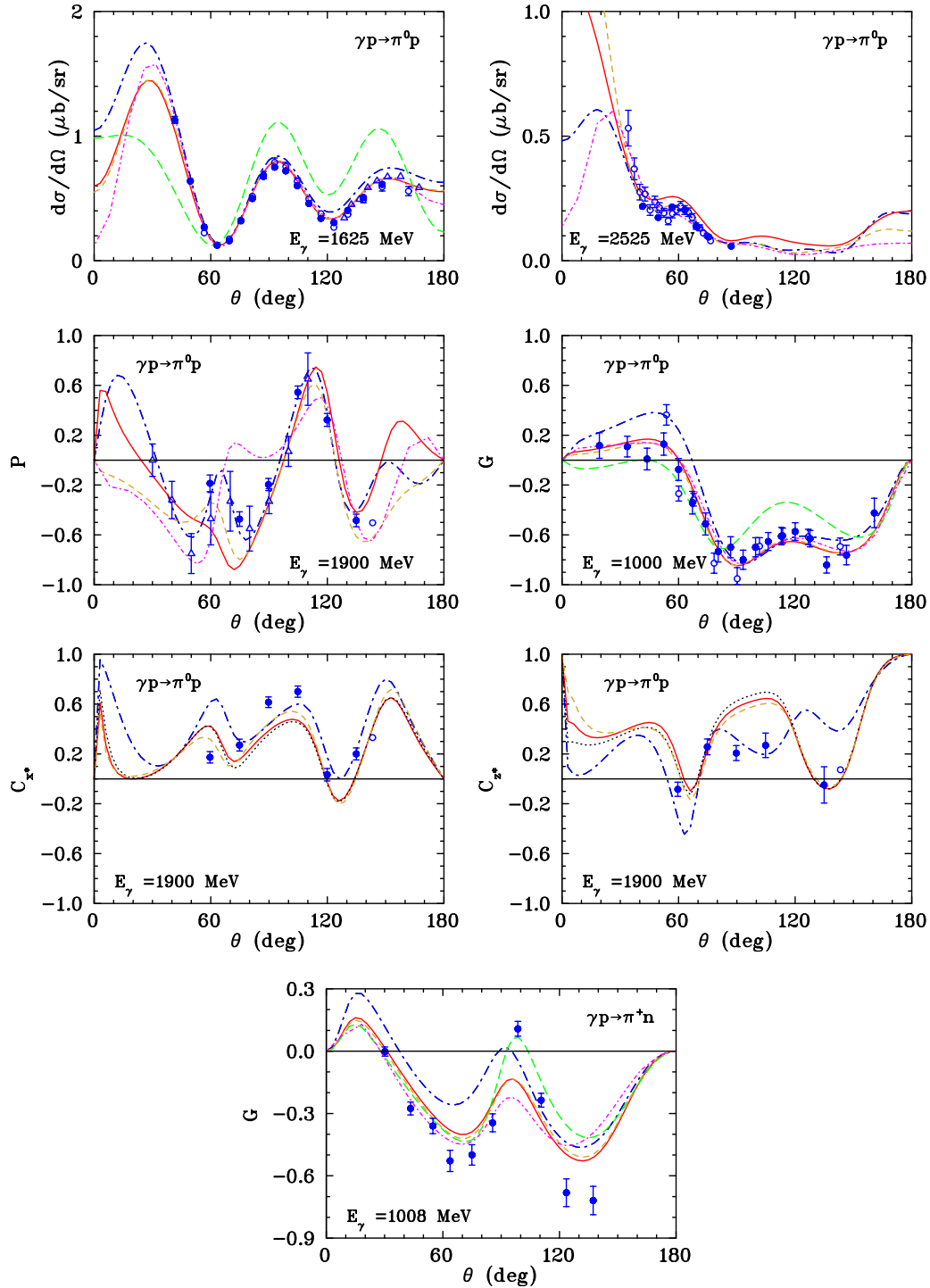
FIG. 1. Samples of pion photoproduction off the proton. Data for $\gamma p \to \pi^0 p$ are from Refs. [42,46,50–52,61,62,66] and for $\gamma p \to \pi^+ n$ are from Ref. [50]. Notation for solutions is given in the caption of Table II. The SAID SM22 (WM22) fit is shown as a red solid (yellow dashed) curve. SAID CM12 [8] (MAID2007 [6]) predictions shown as blue dash-dotted (green dashed) curves. BG2019 [67] predictions are shown as magenta short dash-dotted curves.

amplitude, $E_{2-}^{1/2}$ and $M_{2-}^{1/2}$ (proton target), plus $E_{2-}^{1/2}$ and $M_{2-}^{1/2}$ (neutron target), yielding more self-consistent results.

As in Ref. [38], the fitted partial waves are S_{11}, P_{11}, P_{13}, D_{13}, D_{15}, F_{15}, S_{31}, P_{31}, P_{33}, D_{33}, F_{35}, and F_{37} with pion-nucleon partial waves taken from Ref. [71].

V. RESULTS AND CONCLUSIONS

The present results update the SAID fit (CM12) which first utilized a Chew-Mandelstam K-matrix approach (as opposed to the Heitler K-matrix formalism used in the original SAID analyses). The L + P method for pole parameter extraction
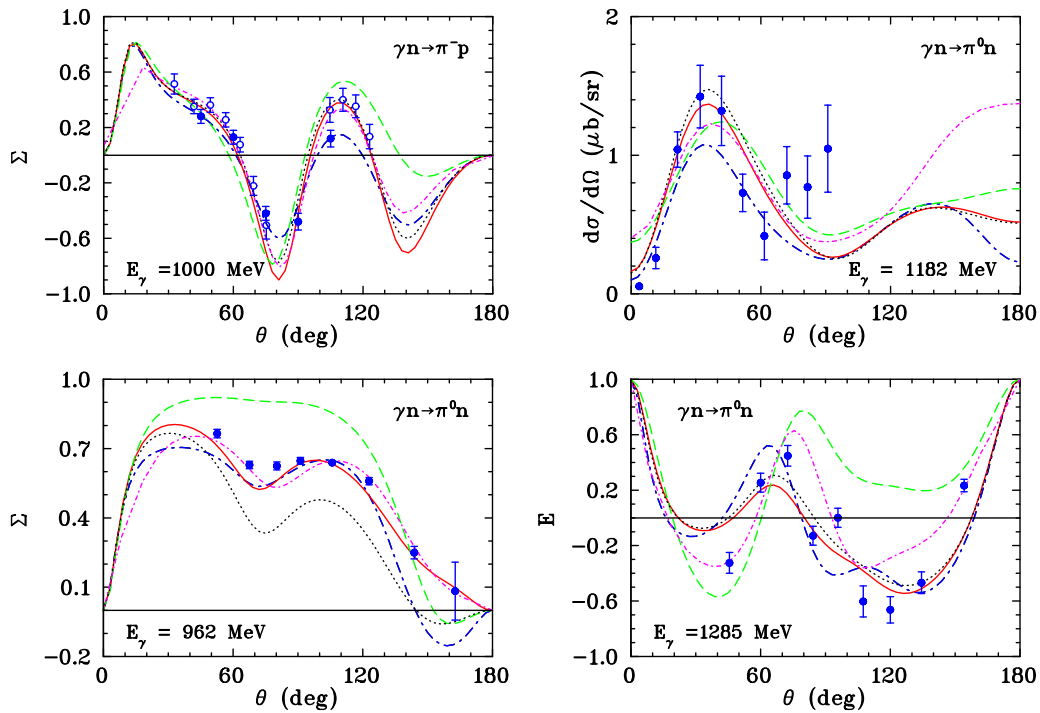
FIG. 2. Samples of pion photoproduction off the neutron. Data for $\gamma n \to \pi^- p$ are from Refs. [56,68] and for $\gamma n \to \pi^0 n$ are from Refs. [58,64,69]. Notation for solutions is given in the caption of Table II. The SAID SM22 (NM22) fit is shown as a red solid (black dotted) curve. SAID CM12 [8] (MAID2007 [6]) predictions are shown as blue dash-dotted (green dashed) curves. BG2019 [67] predictions are shown as magenta short dash-dotted curves.

has been extended to simultaneously incorporate all connected πN elastic and photoproduction amplitudes.

The amplitude tables give pole positions and helicity amplitudes at the pole where available. Values for the $n\gamma$ amplitudes were not extracted in the 2014 SAID analysis; comparisons can now be made to multichannel determinations. Complex amplitudes are given in terms of modulus and phase. In cases where a large phase is found, close to 180 degrees, a minus sign is commonly extracted to ease comparison with the real amplitudes found in older Breit-Wigner fits. The "modulus" then has a sign and a phase closer to zero. Here, however, the modulus remains positive.

In cases where the fitted multipoles have a clear canonical resonance variation, with a relatively small non-resonance contribution, comparison to the Bonn-Gatchina multichannel analysis generally shows good agreement (to the 10% level). This includes the $\Delta(1232)3/2^+$, $N(1520)3/2^-$, $N(1680)5/2^+$, and $\Delta(1905)5/2^+$ and applies to both the $p\gamma$, and $n\gamma$ helicity amplitudes.

Comparisons are more complicated for states associated with the low-angular momentum states $E_{0+}^{1/2}$ and $M_{1-}^{1/2}$. The $N(1535)1/2^-$ and $N(1650)1/2^-$ have some overlap and are close to the ηN threshold cusp. The $N(1440)$ is complicated by the close proximity of its pole position to the $\pi\Delta$ threshold. We note that differences in $N(1535)1/2^-$ $p\gamma$ amplitudes

disappear if one compares instead with the recent Jülich-Bonn analysis [75]. For the $n\gamma$ amplitudes, the agreement is qualitative and no Jülich-Bonn values are available. Qualitative agreement is also seen for the $N(1650)1/2^-$.

Agreement for the $\Delta(1700)3/2^-$ is good for the moduli and at least qualitative for the phases. For the $N(1720)3/2^+$, within fairly large uncertainties, there is qualitative agreement of the helicity amplitude moduli, with less agreement at the level of phases. Hunt and Manley [12] note that the $N(1675)5/2^-$ decays to $p\gamma$ violate the Moorhouse selection rule [76]. We see the moduli of $p\gamma$ photodecay amplitudes to be small but nonzero.

In Figs. 15–17, we display L + P fits for the D_{13} partial-wave and multipole amplitudes, where resonance behavior is clear and the dominant feature, and the S_{11} amplitudes, where resonance overlap and a nearby ηN cusp complicate this process.
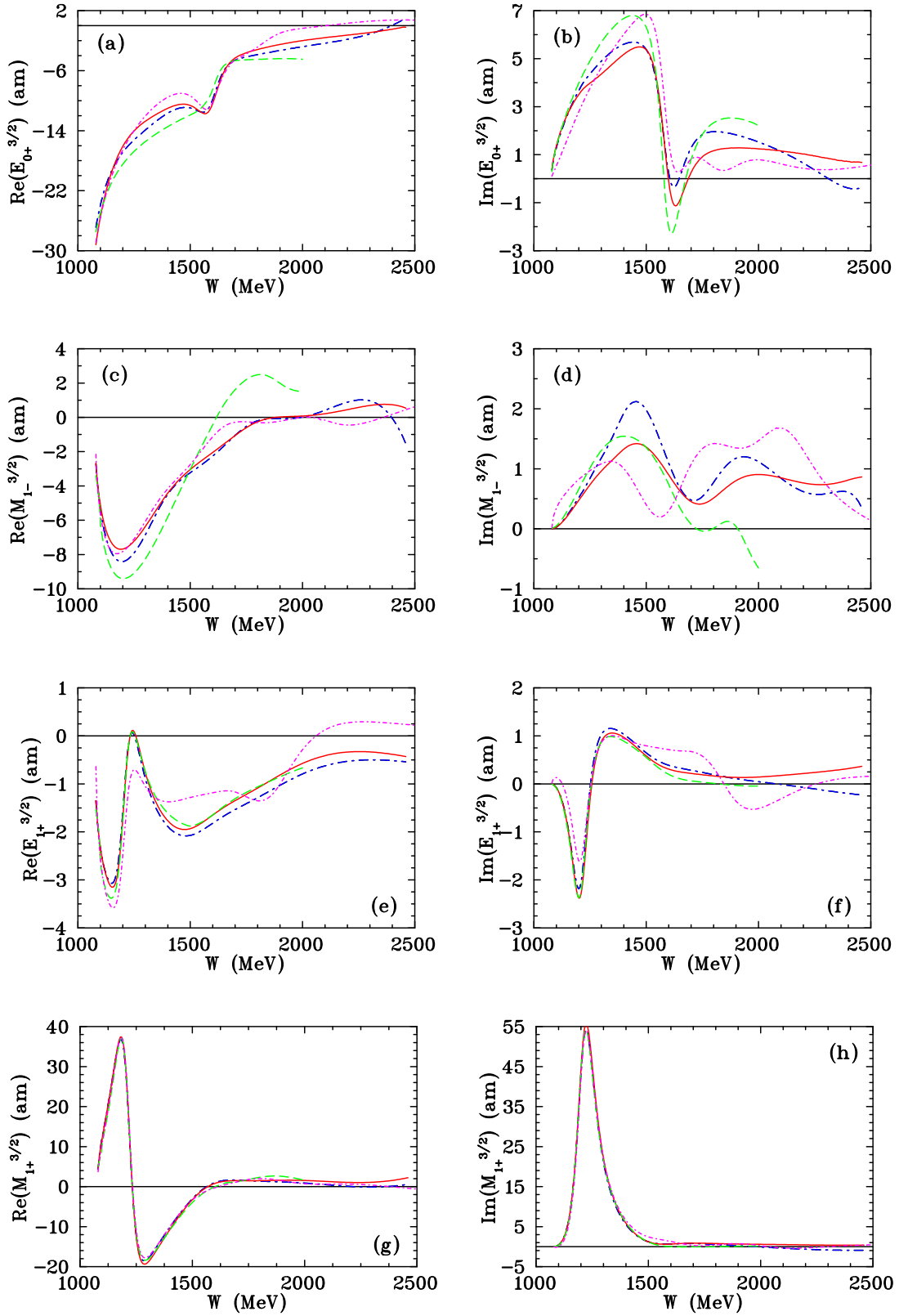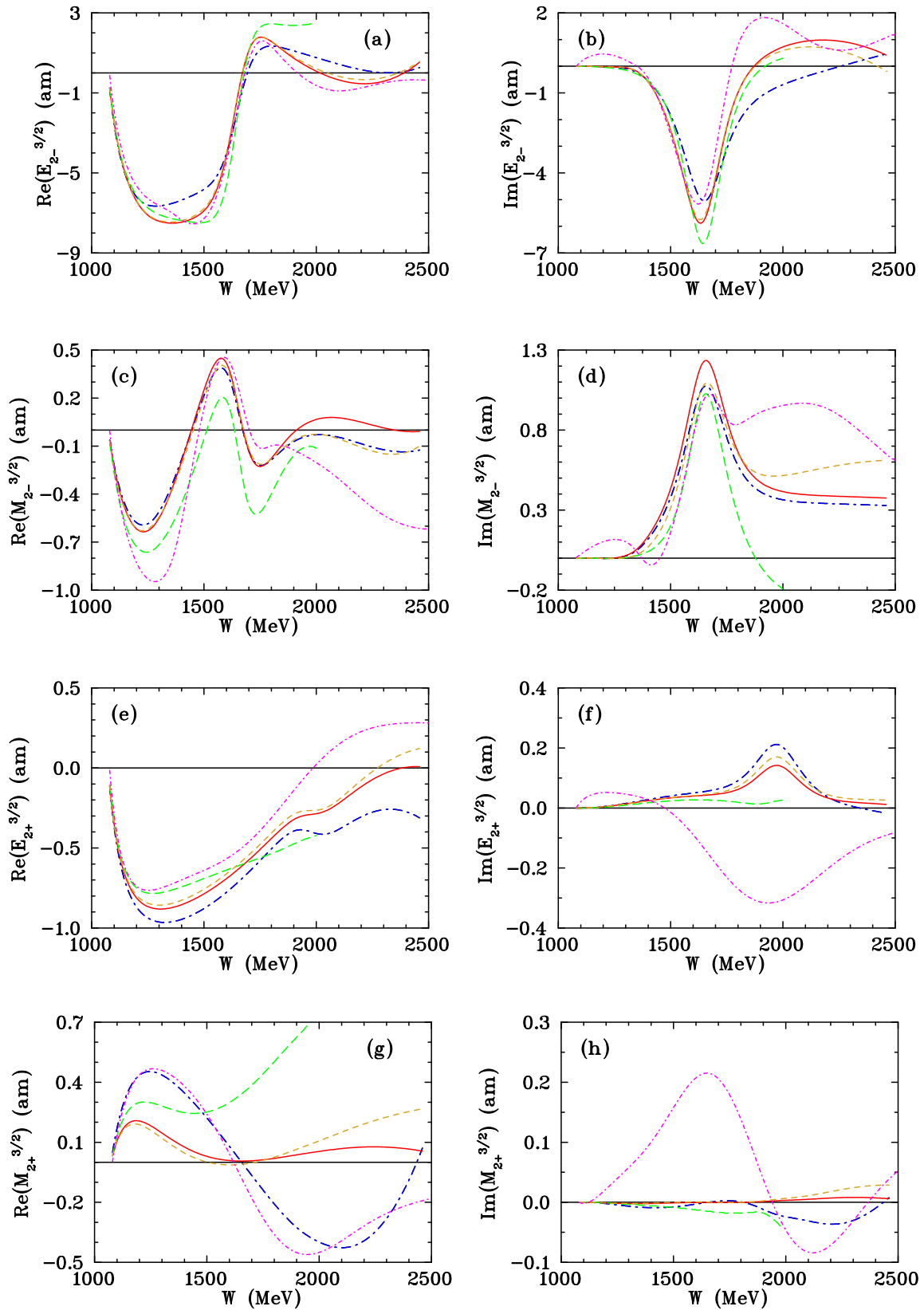
FIG. 3. Comparison $I = 3/2$ multipole amplitudes (orbital momentum $l = 0, 1$) from threshold to $W = 2.5$ GeV ($E_\gamma = 2.7$ GeV). For the amplitudes, the subscript $l\pm$ gives the value of $j = l \pm 1/2$, and the superscript gives the isospin index. Notation for solutions is given in the caption of Table II. New SAID SM22 fit is shown by red solid curves. Previous SAID CM12 [8] (MAID2007 [6], terminates at $W = 2$ GeV) predictions show by blue dash-dotted (green dashed) curves. BG2019 [67] predictions show by magenta short dash-dotted curves.

FIG. 4. Comparison $I = 3/2$ multipole amplitudes (orbital momentum $l = 2$) from threshold to $W = 2.5$ GeV. Notation of the solutions is the same as in Fig. 3. Additionally, the WM22 fit is shown by yellow dashed curves.
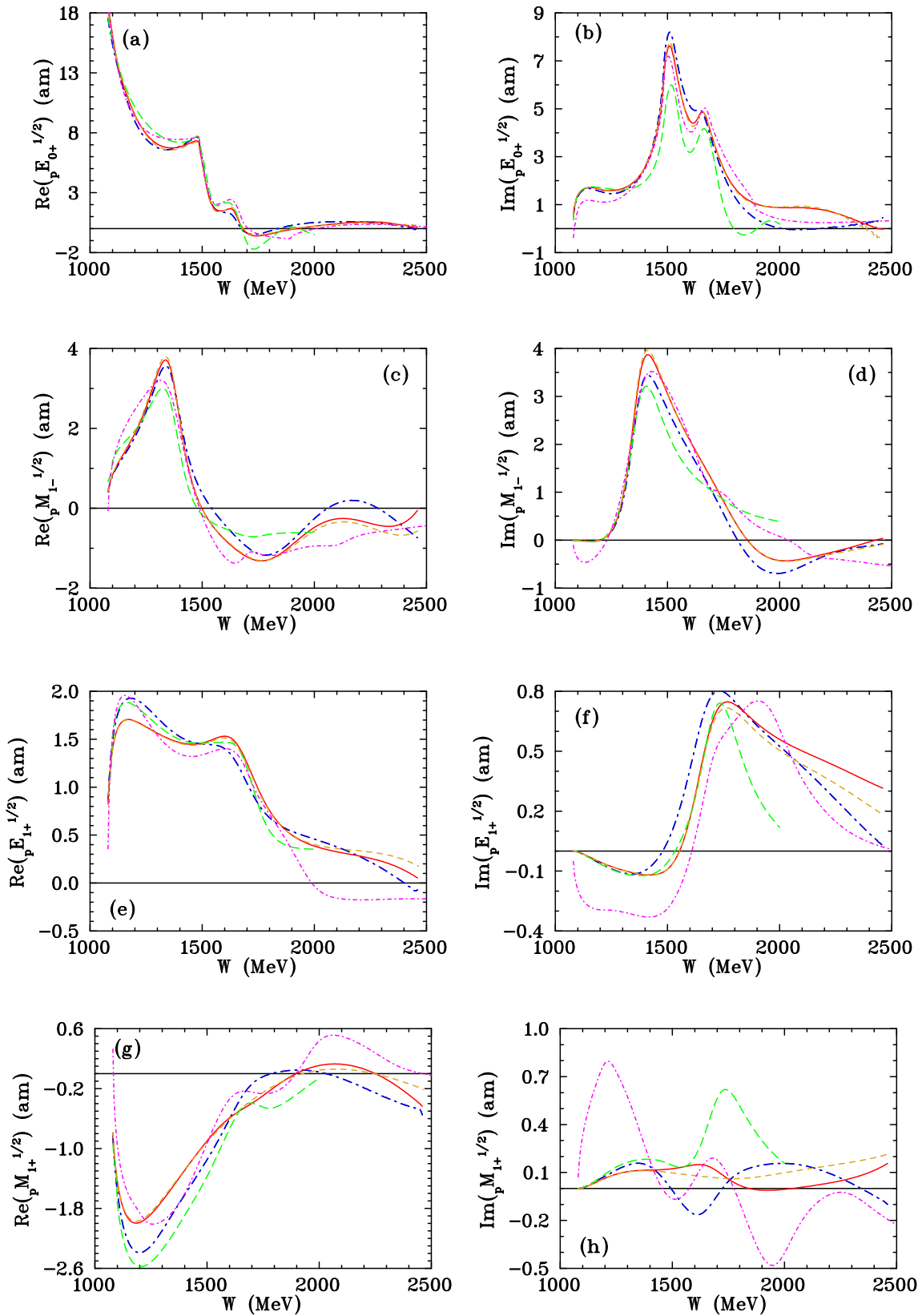
FIG. 5. Comparison proton $I = 1/2$ multipole amplitudes (orbital momentum $l = 0, 1$) from threshold to $W = 2.5$ GeV ($E_\gamma = 2.7$ GeV). Notation of the solutions is the same as in Fig. 3. Additionally, WM22 fit is shown by yellow dashed curves.
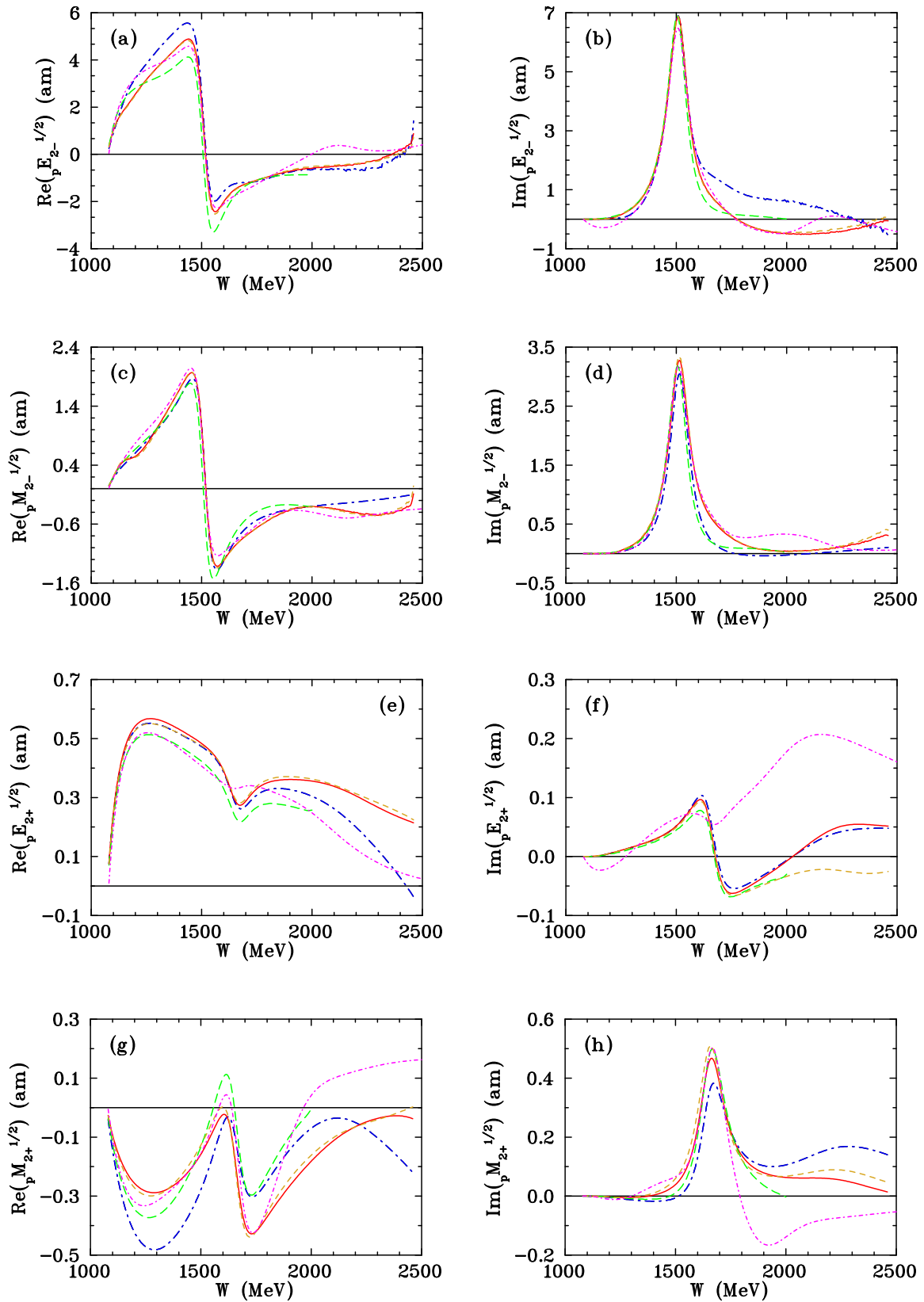
FIG. 6. Comparison of proton $I = 1/2$ multipole amplitudes (orbital momentum $l = 2$) from threshold to $W = 2.5$ GeV. Notation of the solutions is the same as in Fig. 3. For the amplitudes, the subscript p denotes a proton target, Additionally, WM22 fit shown by yellow dashed curves.
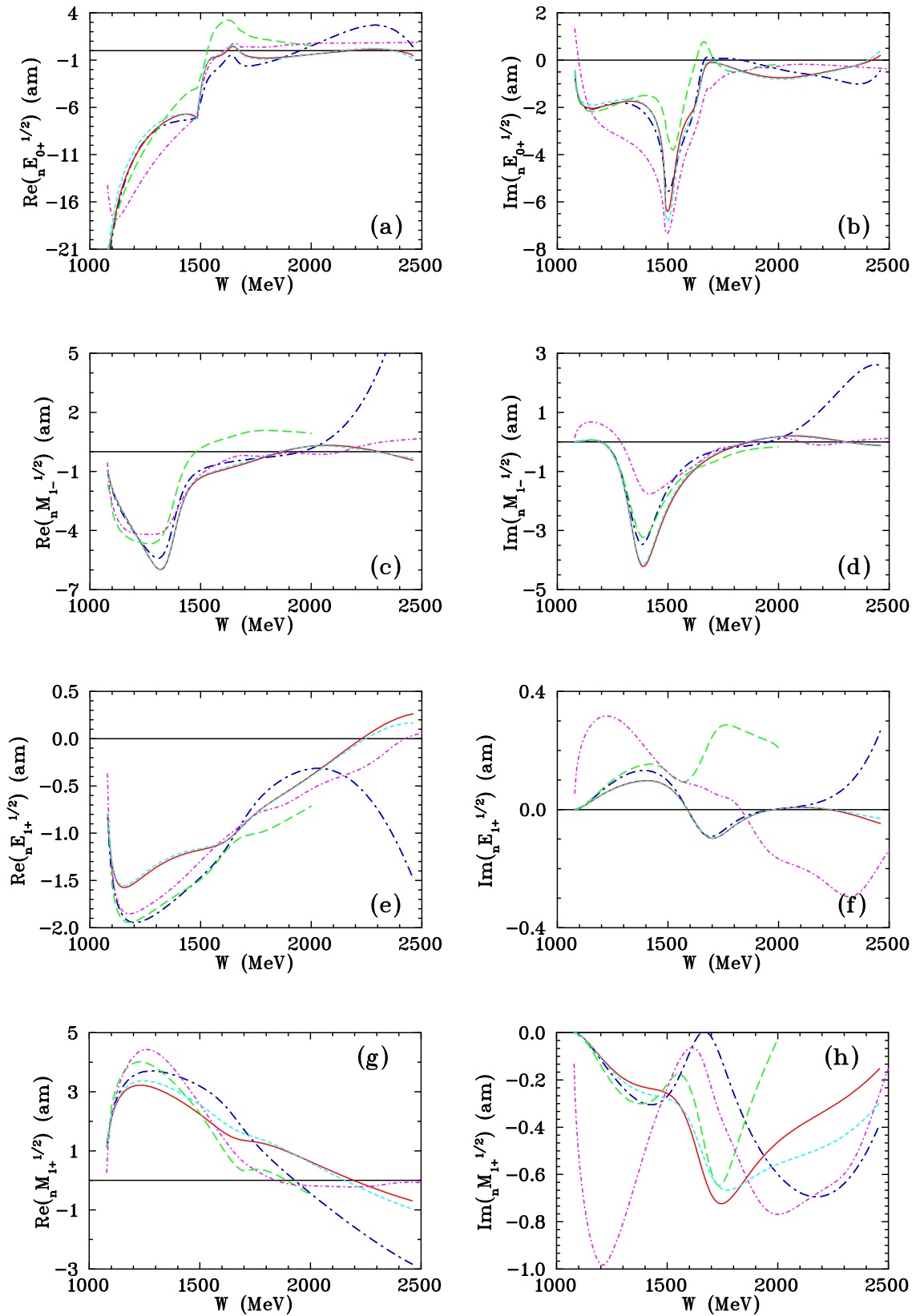
FIG. 7. Comparison of neutron $I = 1/2$ multipole amplitudes (orbital momentum $l = 0, 1$) from threshold to $W = 2.5$ GeV ($E_\gamma = 2.7$ GeV). Notation of the solutions is the same as in Fig. 3. Additionally, cyan short-dashed curves are SM44 fits.
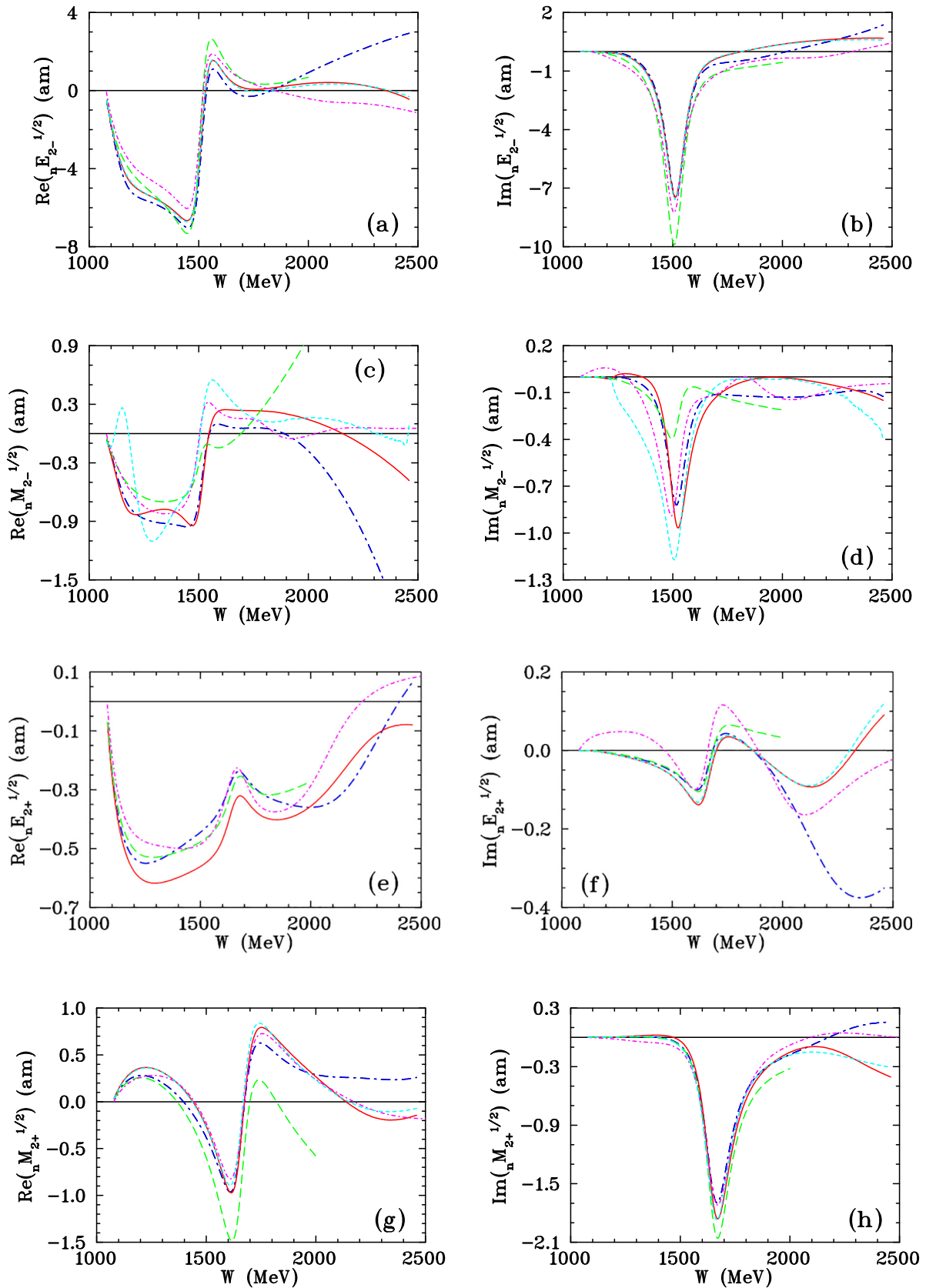
FIG. 8. Comparison neutron $I = 1/2$ multipole amplitudes (orbital momentum $l = 2$) from threshold to $W = 2.5$ GeV. Notation of the solutions is the same as in Fig. 7.
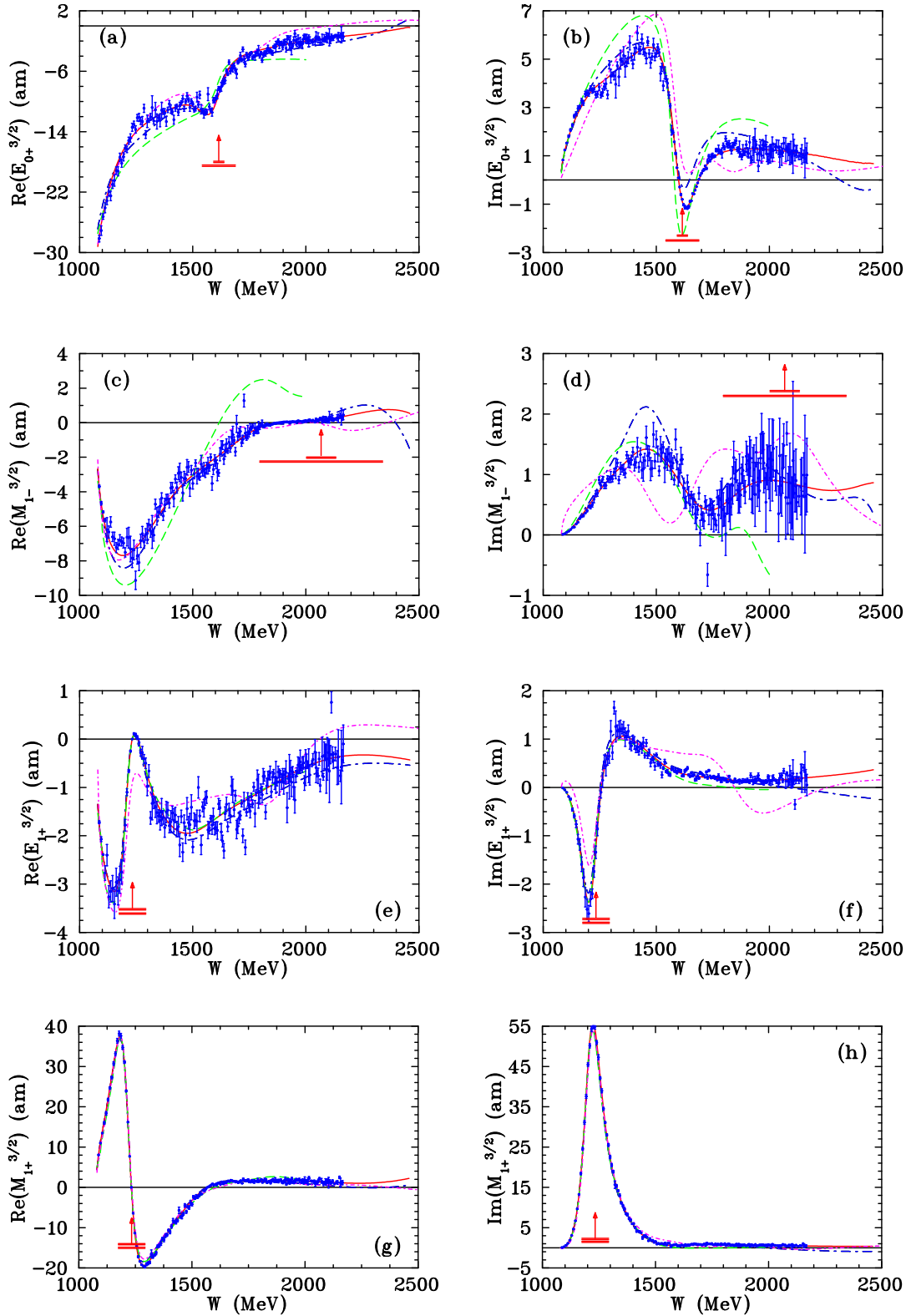
FIG. 9. Comparison of $I = 3/2$ multipole amplitudes (orbital momentum $l = 0, 1$) from threshold to $W = 2.5\,\text{GeV}$ ($E_\gamma = 2.7\,\text{GeV}$). Notation for solutions is given in the caption of Table II. For the amplitudes, the subscript n denotes a neutron target, New SAID SM22 fit is shown by red solid curves. Previous SAID CM12 [8] (MAID2007 [6], terminates at $W = 2\,\text{GeV}$) predictions show by blue dash-dotted (green dashed) curves. BG2019 [67] predictions show by magenta short dash-dotted curves. SE associated with SM22 shown as blue open circles. Vertical arrows indicate resonance energies, W_R, and horizontal bars show full (Γ) and partial ($\Gamma_{\pi N}$) widths associated with the SAID πN solution SP06 (Breit-Wigner parameters) [3].
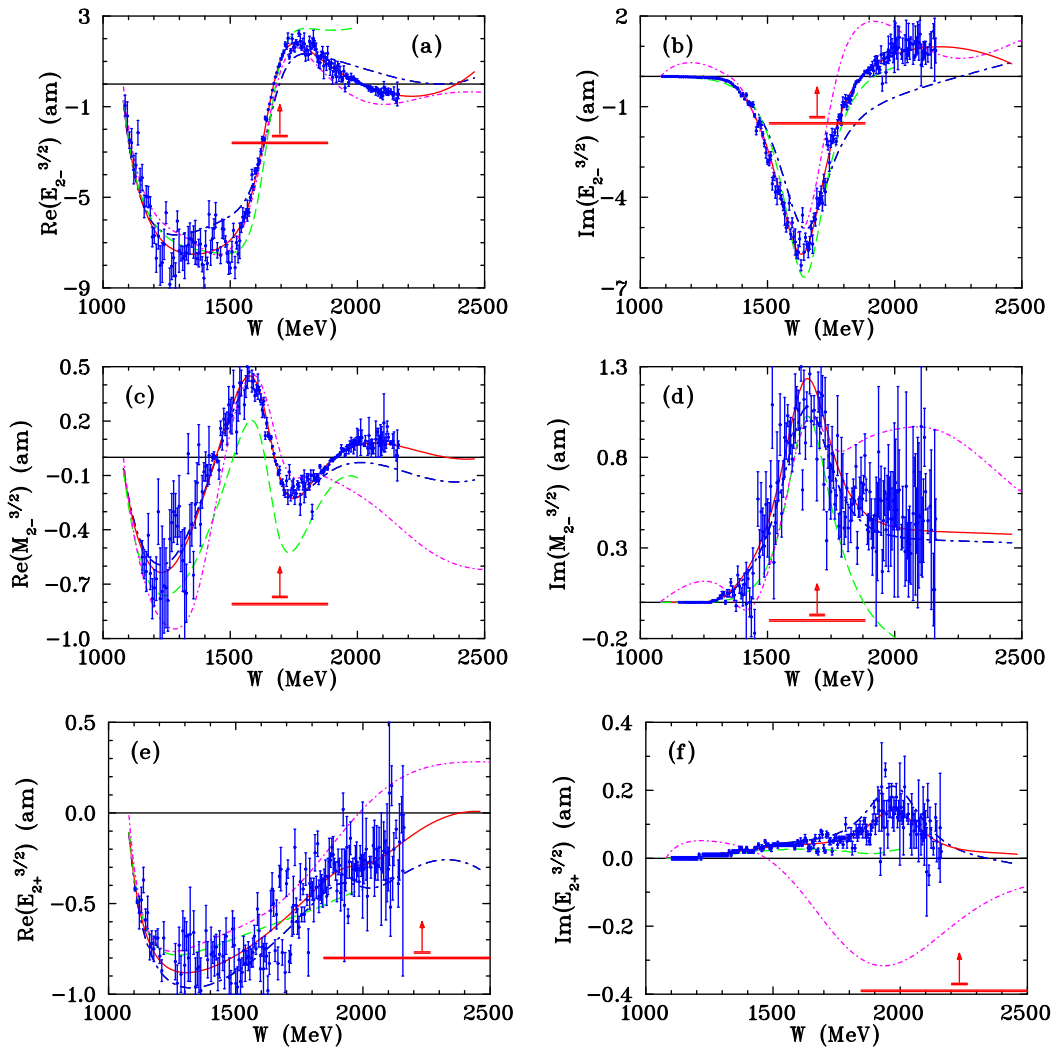
FIG. 10. Comparison $I = 3/2$ multipole amplitudes (orbital momentum $l = 2$) from threshold to $W = 2.5$ GeV. Notation of the solutions and data is the same as in Fig. 9.

FIG. 11. Comparison of proton $I = 1/2$ multipole amplitudes (orbital momentum $l = 0, 1$) from threshold to $W = 2.5$ GeV ($E_\gamma = 2.7$ GeV). Notation of the solutions is the same as in Fig. 9. The blue vertical arrows for (a) and (b) indicate the η production threshold.

FIG. 12. Comparison proton $I = 1/2$ multipole amplitudes (orbital momentum $l = 2$) from threshold to $W = 2.5$ GeV. Notation of the solutions is the same as in Fig. 9.
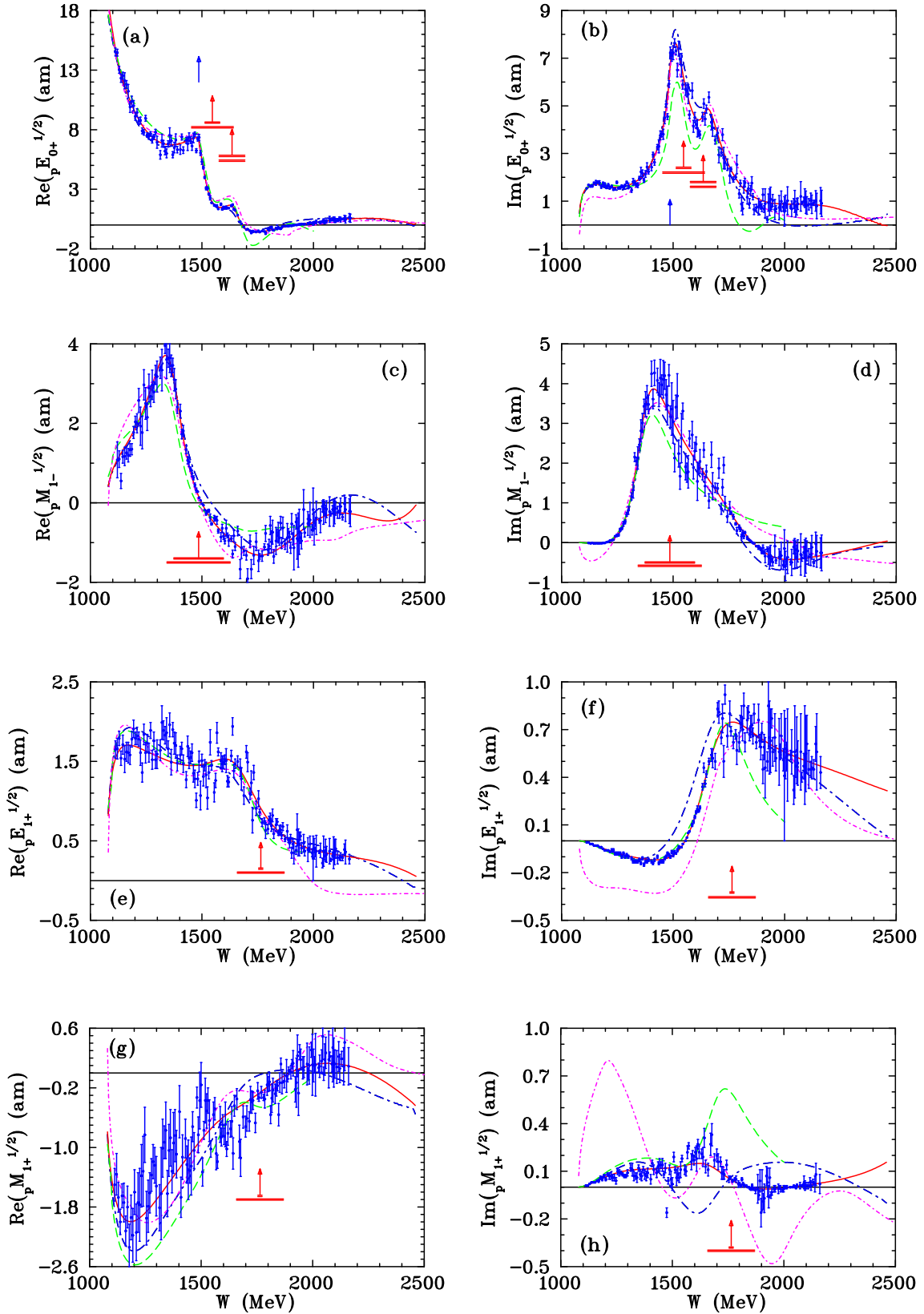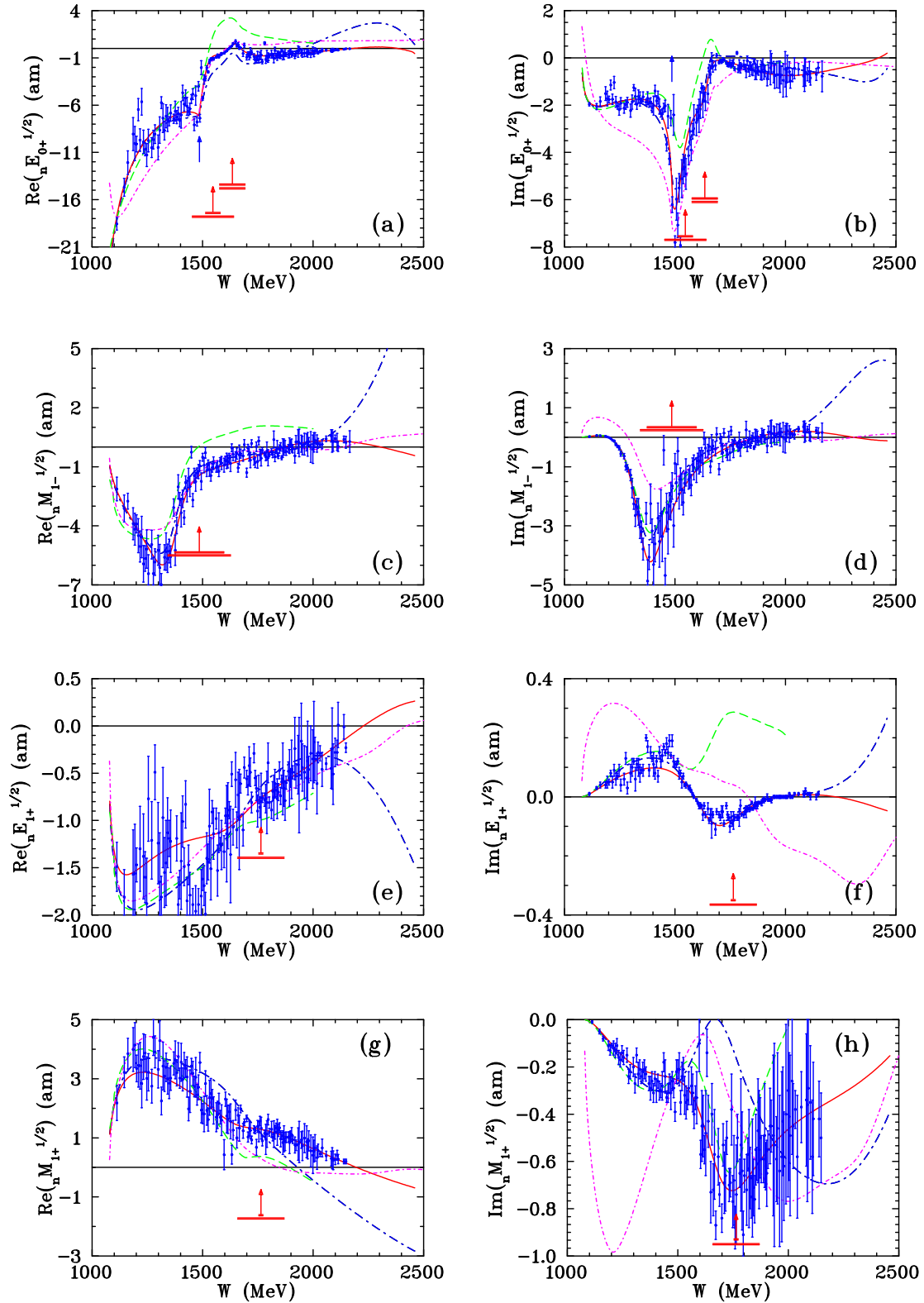
FIG. 13. Comparison neutron $I = 1/2$ multipole amplitudes (orbital momentum $l = 0, 1$) from threshold to $W = 2.5$ GeV ($E_\gamma = 2.7$ GeV). For the amplitudes, the subscript n denotes a neutron target, the subscript $l\pm$ gives the value of $j = l \pm 1/2$, and the superscript gives the isospin index. Notation of the solutions is the same as in Fig. 9. The blue vertical arrows for (a) and (b) indicate the η production threshold.
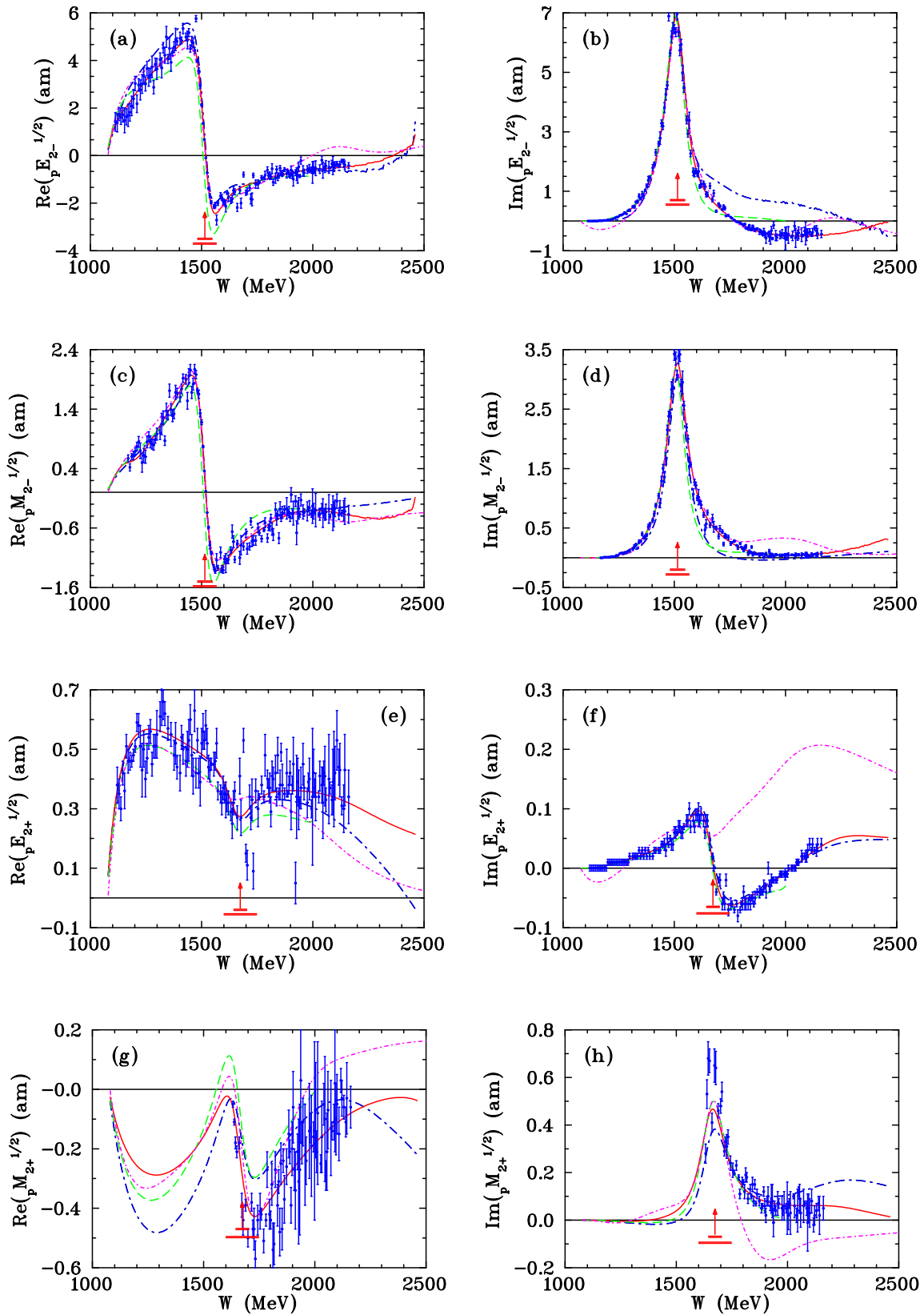
FIG. 14. Comparison of neutron $I = 1/2$ multipole amplitudes (orbital momentum $l = 2$) from threshold to $W = 2.5$ GeV. Notation of the solutions is the same as in Fig. 13.
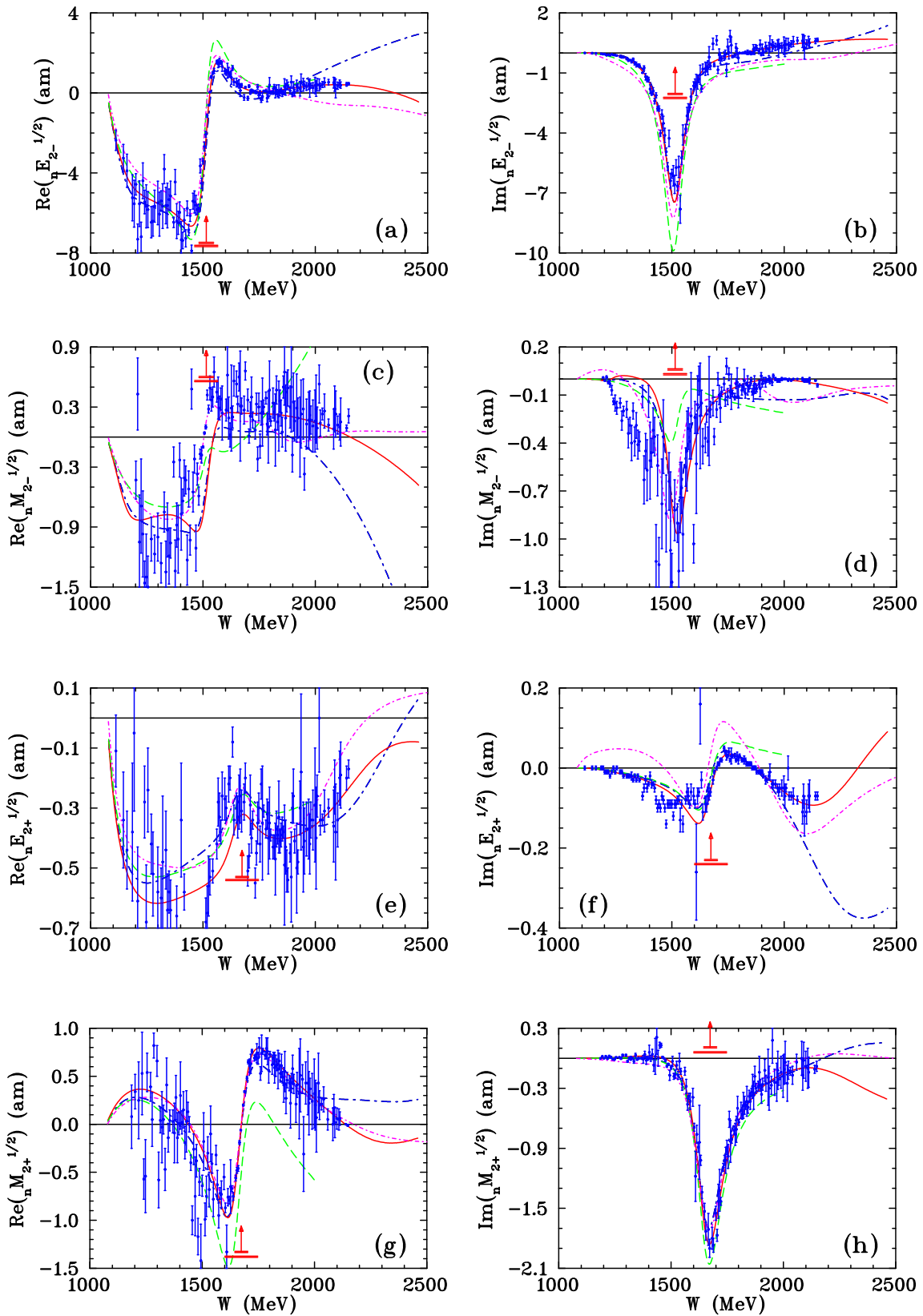
TABLE V. Photon-decay helicity amplitudes at the pole for $p\gamma$ and $n\gamma$ decays. Fit to pion-nucleon elastic amplitude S_{11} and multipole $E_{0+}^{1/2}$. Complex quantities given as modulus and phase. Results from present study (first row), PR2014 [38] (second row), and BnGa [72] (for proton couplings) and [73] (for neutron couplings) (third row).

Resonance	ReW_p (GeV)	$-2ImW_p$ (GeV)	$A_{1/2}(p\gamma)$ (GeV$^{-1/2}$)	Phase (deg)	$A_{1/2}(n\gamma)$ (GeV$^{-1/2}$)	Phase (deg)
$N(1535)1/2^-$	1.500 ± 0.001	0.096 ± 0.006	0.079 ± 0.012	-11.4 ± 1.7	0.067 ± 0.009	-174 ± 22
	1.501 ± 0.006	0.095 ± 0.011	0.074 ± 0.010	-17 ± 11		
	1.500 ± 0.004	0.128 ± 0.009	0.114 ± 0.008	10 ± 5	0.088 ± 0.004	-175 ± 4
$N(1650)1/2^-$	1.650 ± 0.001	0.110 ± 0.008	0.042 ± 0.001	-12.5 ± 0.4	0.026 ± 0.005	-72 ± 13
	1.655 ± 0.011	0.127 ± 0.017	0.041 ± 0.006	16 ± 27		
	1.652 ± 0.007	0.102 ± 0.008	0.032 ± 0.006	-2 ± 11	0.016 ± 0.004	-28 ± 10

TABLE VI. Photon-decay helicity amplitudes at the pole for $p\gamma$ and $n\gamma$ decays. Fit to pion-nucleon elastic amplitude P_{11} and multipole $M_{1-}^{1/2}$. Complex quantities given as modulus and phase. Results from present study (first row), PR2014 [38] (second row), and BnGa [72] (for proton couplings) and [73] (for neutron couplings) (third row).

Resonance	ReW_p (GeV)	$-2ImW_p$ (GeV)	$A_{1/2}(p\gamma)$ (GeV$^{-1/2}$)	Phase (deg)	$A_{1/2}(n\gamma)$ (GeV$^{-1/2}$)	Phase (deg)
$N(1440)1/2^+$	1.358 ± 0.003	0.192 ± 0.005	0.062 ± 0.004	160 ± 11	0.080 ± 0.005	1.25 ± 0.08
	1.360 ± 0.005	0.183 ± 0.019	0.055 ± 0.003	167 ± 11		
	1.369 ± 0.003	0.189 ± 0.005	0.044 ± 0.005	140 ± 8	0.041 ± 0.005	23 ± 10

TABLE VII. Photon-decay helicity amplitudes at the pole for $p\gamma$ and $n\gamma$ decays. Fit to pion-nucleon elastic amplitude P_{13} and multipoles $E_{1+}^{1/2}$ and $M_{1+}^{1/2}$. Complex quantities given as modulus and phase. Results from present study (first row), PR2014 [38] (second row), and BnGa [72] (for proton couplings) and [73] (for neutron couplings) (third row).

Resonance	ReW_p (GeV)	$-2ImW_p$ (GeV)	$A_{1/2}(p\gamma)$ (GeV$^{-1/2}$)	Phase (deg)	$A_{3/2}(p\gamma)$ (GeV$^{-1/2}$)	Phase (deg)	$A_{1/2}(n\gamma)$ (GeV$^{-1/2}$)	Phase (deg)	$A_{3/2}(n\gamma)$ (GeV$^{-1/2}$)	Phase (deg)
$N(1720)3/2^+$	1.670 ± 0.001	0.280 ± 0.002	0.057 ± 0.027	-42 ± 19	0.071 ± 0.033	-8 ± 4	0.056 ± 0.021	-21 ± 8	0.065 ± 0.024	169 ± 64
	1.651 ± 0.009	0.311 ± 0.045	0.059 ± 0.002	-14 ± 8	0.045 ± 0.005	-151 ± 11				
	1.670 ± 0.025	0.430 ± 0.100	0.115 ± 0.045	0 ± 35	0.140 ± 0.040	65 ± 35	$0.025^{+0.040}_{-0.015}$	105 ± 35	0.100 ± 0.035	-80 ± 35

TABLE VIII. Photon-decay helicity amplitudes at the pole for $p\gamma$ and $n\gamma$ decays. Fit to pion-nucleon elastic amplitude D_{13} and multipoles $E_{2-}^{1/2}$ and $M_{2-}^{1/2}$. Complex quantities given as modulus and phase. Results from present study (first row), PR2014 [38] (second row), and BnGa [72] (for proton couplings) and [73] (for neutron couplings) (third row).

Resonance	ReW_p (GeV)	$-2ImW_p$ (GeV)	$A_{1/2}(p\gamma)$ (GeV$^{-1/2}$)	Phase (deg)	$A_{3/2}(p\gamma)$ (GeV$^{-1/2}$)	Phase (deg)	$A_{1/2}(n\gamma)$ (GeV$^{-1/2}$)	Phase (deg)	$A_{3/2}(n\gamma)$ (GeV$^{-1/2}$)	Phase (deg)
$N(1520)3/2^-$	1.511 ± 0.001	0.116 ± 0.002	0.029 ± 0.001	156 ± 8	0.144 ± 0.007	4.0 ± 0.2	0.044 ± 0.004	-175 ± 15	0.121 ± 0.010	-170 ± 14
	1.514 ± 0.001	0.109 ± 0.005	0.028 ± 0.001	154 ± 7	0.133 ± 0.006	13 ± 2				
	1.507 ± 0.002	0.111 ± 0.003	0.023 ± 0.004	174 ± 5	0.131 ± 0.006	4 ± 4	0.045 ± 0.005	175 ± 4	0.119 ± 0.005	-175 ± 4

TABLE IX. Photon-decay helicity amplitudes at the pole for $p\gamma$ and $n\gamma$ decays. Fit to pion-nucleon elastic amplitude D_{15} and multipoles $E_{2+}^{1/2}$ and $M_{2+}^{1/2}$. Complex quantities given as modulus and phase. Results from present study (first row), PR2014 [38] (second row), and BnGa [72] (for proton couplings) and [73] (for neutron couplings) (third row).

Resonance	ReW_p (GeV)	$-2ImW_p$ (GeV)	$A_{1/2}(p\gamma)$ (GeV$^{-1/2}$)	Phase (deg)	$A_{3/2}(p\gamma)$ (GeV$^{-1/2}$)	Phase (deg)	$A_{1/2}(n\gamma)$ (GeV$^{-1/2}$)	Phase (deg)	$A_{3/2}(n\gamma)$ (GeV$^{-1/2}$)	Phase (deg)
$N(1675)5/2^-$	1.658 ± 0.003	0.141 ± 0.005	0.020 ± 0.006	165 ± 43	0.020 ± 0.005	23 ± 6	0.123 ± 0.027	-19 ± 4	0.084 ± 0.018	-170 ± 38
	1.657 ± 0.005	0.141 ± 0.011	0.015 ± 0.002	25 ± 12	0.019 ± 0.002	-40 ± 8				
	1.655 ± 0.004	0.147 ± 0.005	0.022 ± 0.003	-12 ± 7	0.028 ± 0.006	-17 ± 6	0.053 ± 0.004	177 ± 5	0.073 ± 0.005	168 ± 5

TABLE X. Photon-decay helicity amplitudes at the pole for $p\gamma$ and $n\gamma$ decays. Fit to pion-nucleon elastic amplitude F_{15} and multipoles $E_{3-}^{1/2}$ and $M_{3-}^{1/2}$. Complex quantities given as modulus and phase. Results from present study (first row), PR2014 [38] (second row), and BnGa [72] (for proton couplings) and [73] (for neutron couplings) (third row).

Resonance	ReW_p (GeV)	$-2ImW_p$ (GeV)	$A_{1/2}(p\gamma)$ (GeV$^{-1/2}$)	Phase (deg)	$A_{3/2}(p\gamma)$ (GeV$^{-1/2}$)	Phase (deg)	$A_{1/2}(n\gamma)$ (GeV$^{-1/2}$)	Phase (deg)	$A_{3/2}(n\gamma)$ (GeV$^{-1/2}$)	Phase (deg)
$N(1680)5/2^+$	1.672 ± 0.017	0.113 ± 0.004	0.020 ± 0.002	141 ± 25	0.126 ± 0.011	-1.1 ± 0.1	0.037 ± 0.006	-15 ± 3	0.040 ± 0.007	-176 ± 29
	1.674 ± 0.003	0.113 ± 0.005	0.014 ± 0.005	130 ± 20	0.123 ± 0.004	-6 ± 3				
	1.678 ± 0.005	0.113 ± 0.004	0.013 ± 0.003	160 ± 17	0.135 ± 0.005	1 ± 3	0.032 ± 0.003	-7 ± 5	0.063 ± 0.004	170 ± 5

TABLE XI. Photon-decay helicity amplitudes at the pole for $p\gamma$ decay. Fit to pion-nucleon elastic amplitude P_{33} multipoles $E_{1+}^{3/2}$ and $M_{1+}^{3/2}$ and amplitude S_{31} multipoles $E_{0+}^{3/2}$. Complex quantities given as modulus and phase. Results from present study (first row), PR2014 [38] (second row), and BnGa [74] [for $\Delta(1232)3/2^+$] and [72] [for $\Delta(1620)1/2^-$] (third row).

Resonance	ReW_p (GeV)	$-2ImW_p$ (GeV)	$A_{1/2}(p\gamma)$ (GeV$^{-1/2}$)	Phase (deg)	$A_{3/2}(p\gamma)$ (GeV$^{-1/2}$)	Phase (deg)
$\Delta(1232)3/2^+$	1.210 ± 0.001	0.995 ± 0.001	0.130 ± 0.005	161 ± 7	0.263 ± 0.012	171 ± 8
	1.211 ± 0.001	0.101 ± 0.002	0.129 ± 0.002	167 ± 2	0.259 ± 0.002	179 ± 2
	1.210 ± 0.001	0.099 ± 0.002	0.131 ± 0.004	161 ± 2	0.254 ± 0.005	171 ± 1
$\Delta(1620)1/2^-$	1.594 ± 0.003	0.128 ± 0.006	0.0594 ± 0.0002	-2 ± 13		
	1.596 ± 0.003	0.124 ± 0.007	0.051 ± 0.001	4 ± 9		
	1.597 ± 0.005	0.134 ± 0.008	0.054 ± 0.007	-6 ± 7		

TABLE XII. Photon-decay helicity amplitudes at the pole for $p\gamma$ decay. Fit to pion-nucleon elastic amplitude D_{33} and multipoles $E_{2-}^{3/2}$ and $M_{2-}^{3/2}$. Complex quantities given as modulus and phase. Results from present study (first row), PR2014 [38] (second row), and BnGa [72] (third row).

Resonance	ReW_p (GeV)	$-2ImW_p$ (GeV)	$A_{1/2}(p\gamma)$ (GeV$^{-1/2}$)	Phase (deg)	$A_{3/2}(p\gamma)$ (GeV$^{-1/2}$)	Phase (deg)
$\Delta(1700)3/2^-$	1.638 ± 0.002	0.267 ± 0.004	0.147 ± 0.004	12.0 ± 0.3	0.173 ± 0.004	25.8 ± 0.6
	1.650 ± 0.004	0.255 ± 0.011	0.125 ± 0.002	20 ± 2	0.132 ± 0.004	27 ± 3
	1.685 ± 0.010	0.300 ± 0.015	0.175 ± 0.020	50 ± 10	0.180 ± 0.020	45 ± 10

TABLE XIII. Photon-decay helicity amplitudes at the pole for $p\gamma$ decay. Fit to pion-nucleon elastic amplitude F_{35} multipoles $E_{3-}^{3/2}$ and $M_{3-}^{3/2}$ and amplitude P_{31} multipoles $M_{1-}^{3/2}$. Complex quantities given as modulus and phase. Results from present study (first row), PR2014 [38] (second row), and BnGa [72] (third row).

Resonance	ReW_p (GeV)	$-2ImW_p$ (GeV)	$A_{1/2}(p\gamma)$ (GeV$^{-1/2}$)	Phase (deg)	$A_{3/2}(p\gamma)$ (GeV$^{-1/2}$)	Phase (deg)
$\Delta(1905)5/2^+$	1.799 ± 0.006	0.227 ± 0.012	0.051 ± 0.006	166 ± 21	0.009 ± 0.001	-171 ± 22
	1.817 ± 0.007	0.257 ± 0.015	0.015 ± 0.002	-29 ± 9	0.038 ± 0.001	-174 ± 2
	1.800 ± 0.006	0.290 ± 0.015	0.025 ± 0.005	-28 ± 12	0.050 ± 0.004	-175 ± 10
$\Delta(1910)1/2^+$	1.756 ± 0.014	0.412 ± 0.031	0.037 ± 0.001	138 ± 59		
	1.778 ± 0.020	0.394 ± 0.040	0.033 ± 0.005	177 ± 11		
	1.840 ± 0.040	0.370 ± 0.060	0.027 ± 0.009	-33 ± 60		

TABLE XIV. Photon-decay helicity amplitudes at the pole for $p\gamma$ decay. Fit to pion-nucleon elastic amplitude F_{37} and multipoles $E_{3+}^{3/2}$ and $M_{3+}^{3/2}$. Complex quantities given as modulus and phase. Results from present study (first row), PR2014 [38] (second row), and BnGa [72] (third row).

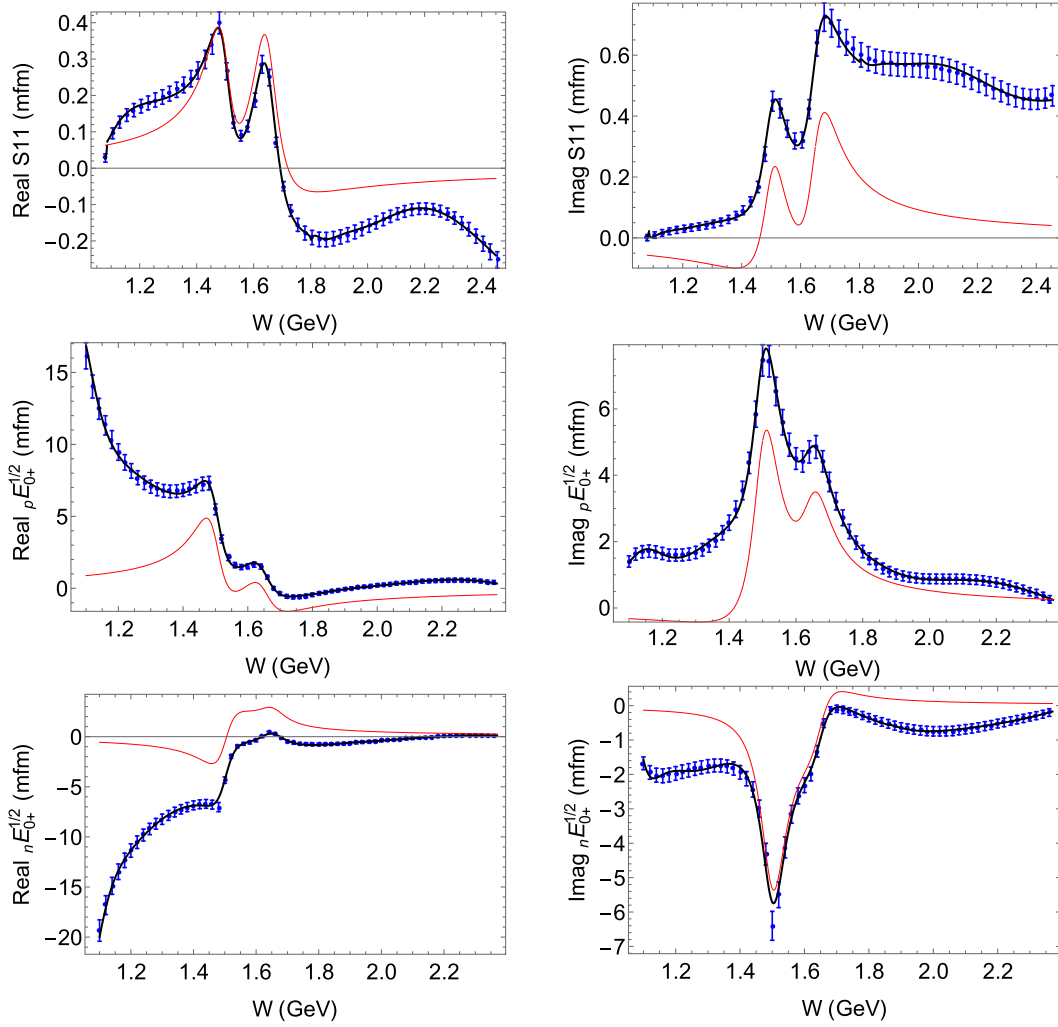| Resonance	ReW_p (GeV)	$-2ImW_p$ (GeV)	$A_{1/2}(p\gamma)$ (GeV$^{-1/2}$)	Phase (deg)	$A_{3/2}(p\gamma)$ (GeV$^{-1/2}$)	Phase (deg)
$\Delta(1950)7/2^+$	1.883 ± 0.002	0.240 ± 0.005	0.072 ± 0.008	179 ± 20	0.090 ± 0.010	173 ± 19
	1.879 ± 0.005	0.231 ± 0.009	0.076 ± 0.004	175 ± 4	0.095 ± 0.005	-178 ± 4
	1.888 ± 0.004	0.245 ± 0.008	0.067 ± 0.004	170 ± 5	0.095 ± 0.004	170 ± 5

FIG. 15. Samples of Laurent + Pietarinen (L + P) coupled fit of the S_{11} πN partial wave of the GWU-SAID fit WI08 [71] and the SM22 ED GWU-SAID multipole solutions. Blue symbols are the GWU-SAID solutions, solid black curves are the L + P coupled-multipole fit, and thin red curves are the resonant contribution in the L + P coupled-multipole fit.
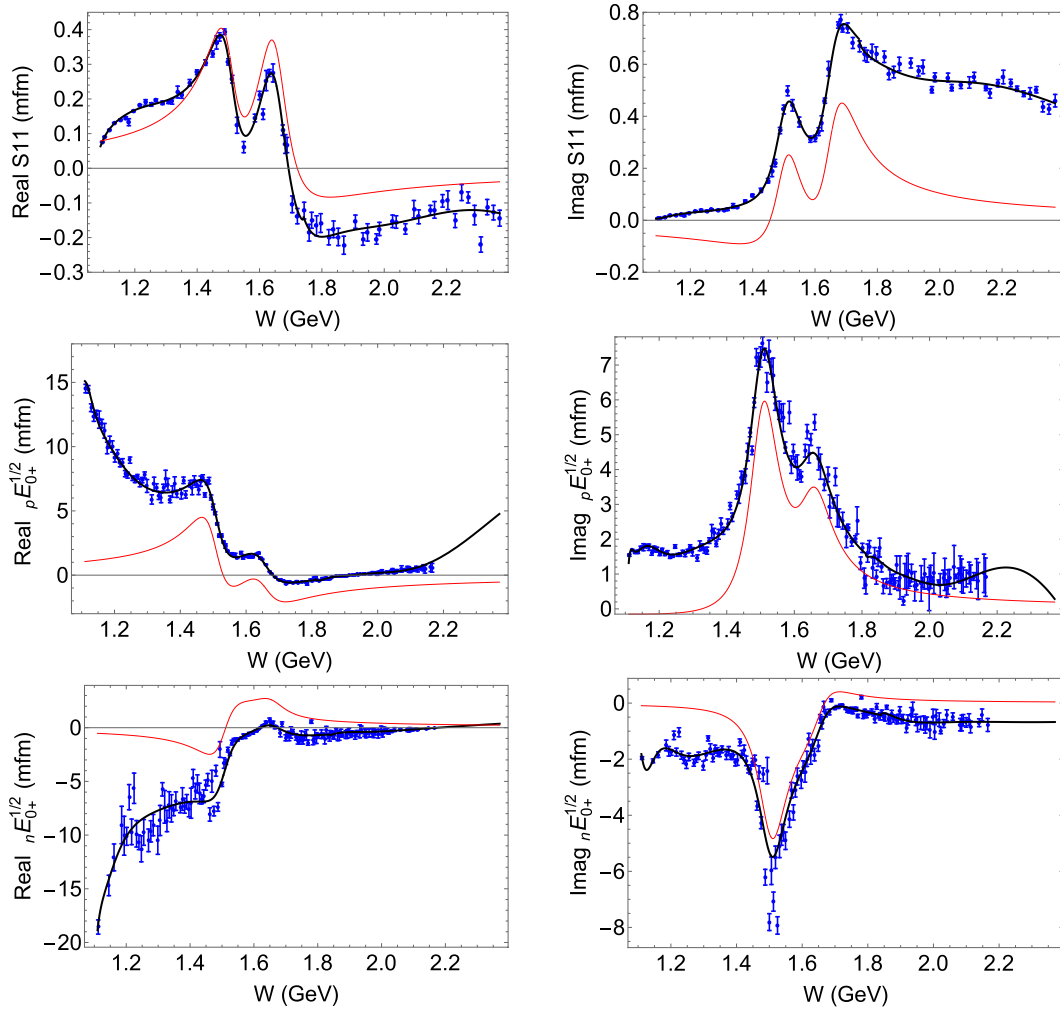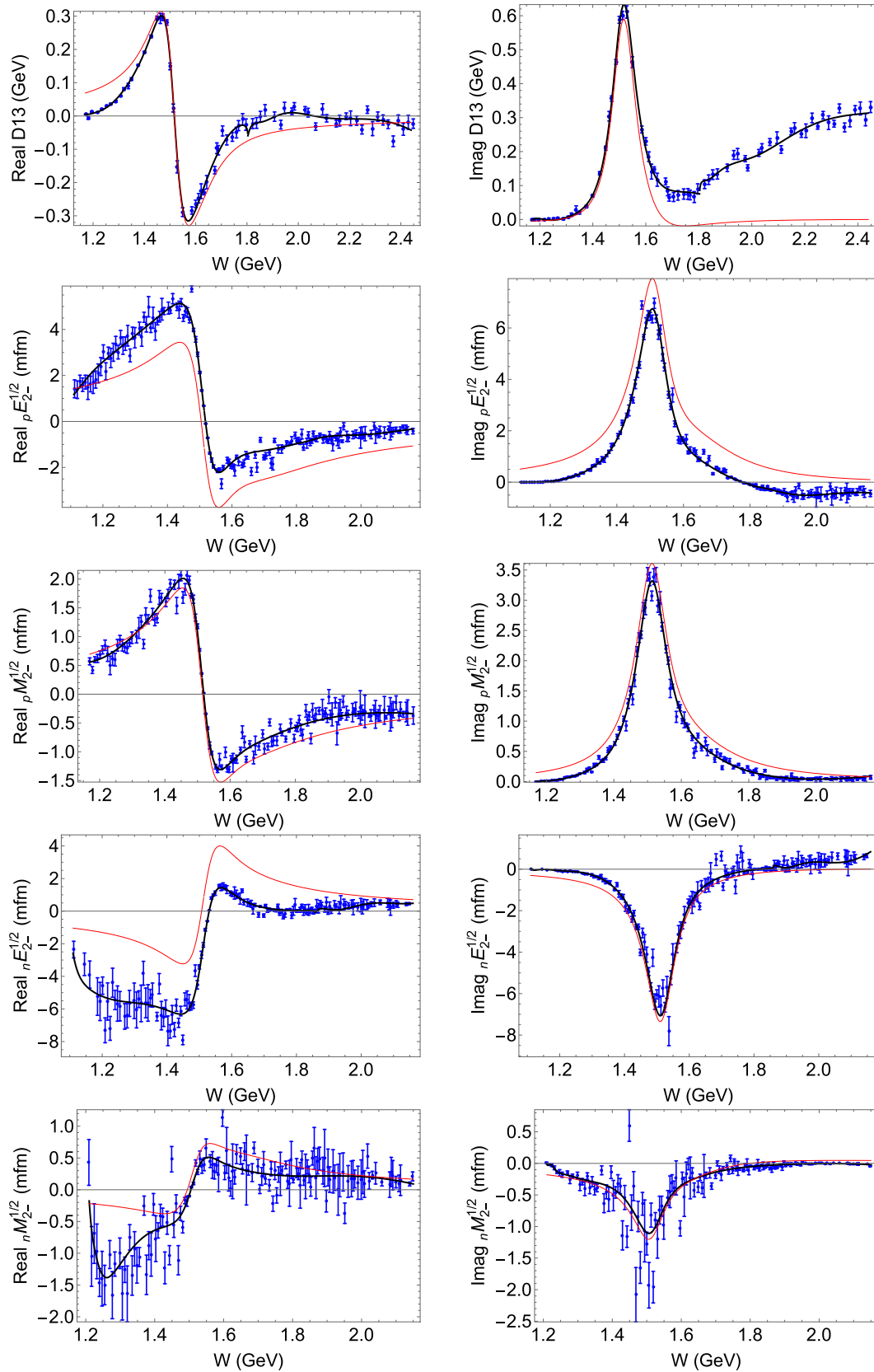
FIG. 16. Samples of Laurent + Pietarinen (L + P) coupled fit of the S_{11} πN partial wave of the GWU-SAID fit WI08 [71] and SM22 SE4 GWU-SAID multipole solutions. Notation of the solutions is the same as in Fig. 15.

FIG. 17. Samples of Laurent + Pietarinen (L + P) coupled fit of the D_{13} πN partial wave of the GWU-SAID fit WI08 [71] and SM22 SE4 GWU-SAID multipole solutions. Notation of the solutions is the same as in Fig. 15.

[1] R. L. Workman *et al.* (Particle Data Group), Review of particle physics, Prog. Theor. Exp. Phys. (2022) 083C01.

[2] G. Höhler, *Pion Nucleon Scattering. Part 2 Methods and Results of Phenomenological Analyses*, Landolt-Boernstein - Group I Elementary Particles, Nuclei and Atoms 9B2 (Springer-Verlag, 1983).

[3] R. A. Arndt, W. J. Briscoe, I. I. Strakovsky, and R. L. Workman, Extended partial-wave analysis of πN scattering data, Phys. Rev. C **74**, 045205 (2006).

[4] R. E. Cutkosky, R. E. Hendrick, J. W. Alcock, Y. A. Chao, R. G. Lipes, J. C. Sandusky, and R. L. Kelly, Pion-nucleon partial wave analysis, Phys. Rev. D **20**, 2804 (1979).

[5] M. Shrestha and D. M. Manley, Multichannel parametrization of πN scattering amplitudes and extraction of resonance parameters, Phys. Rev. C **86**, 055203 (2012).

[6] D. Drechsel, S. S. Kamalov, and L. Tiator, Unitary Isobar model - MAID2007, Eur. Phys. J. A **34**, 69 (2007); the MAID analyses are available through the Mainz web-site: http://wwwkph.uni-mainz.de/MAID/.

[7] I. G. Aznauryan, Multipole amplitudes of pion photoproduction on nucleons up to 2-Gev within dispersion relations and unitary isobar model, Phys. Rev. C **67**, 015209 (2003)

[8] R. L. Workman, M. W. Paris, W. J. Briscoe, and I. I. Strakovsky, Unified Chew-Mandelstam SAID analysis of pion photoproduction data, Phys. Rev. C **86**, 015202 (2012).

[9] O. Hanstein, D. Drechsel, and L. Tiator, Multipole analysis of pion photoproduction based on fixed t dispersion relations and unitarity, Nucl. Phys. A **632**, 561 (1998).

[10] A. V. Anisovich, E. Klempt, V. A. Nikonov, M. A. Matveev, A. V. Sarantsev, and U. Thoma, Photoproduction of pions and properties of baryon resonances from a Bonn-Gatchina partial wave analysis, Eur. Phys. J. A **44**, 203 (2010).

[11] H. Kamano, S. X. Nakamura, T. S. H. Lee, and T. Sato, Isospin decomposition of $\gamma N \to N^*$ transitions within a dynamical coupled-channels model, Phys. Rev. C **94**, 015201 (2016).

[12] B. C. Hunt and D. M. Manley, Updated determination of N^* resonance parameters using a unitary, multichannel formalism, Phys. Rev. C **99**, 055205 (2019).

[13] J. Nys, J. Ryckebusch, D. G. Ireland, and D. I. Glazier, Model discrimination in pseudoscalar-meson photoproduction, Phys. Lett. B **759**, 260 (2016).

[14] D. Rönchen, M. Döring, and U. G. Meißner, The impact of $K^+\Lambda$ photoproduction on the resonance spectrum, Eur. Phys. J. A **54**, 110 (2018).

[15] A. M. Sandorfi, S. Hoblit, H. Kamano, and T. S. H. Lee, Determining pseudoscalar meson photo-production amplitudes from complete experiments, J. Phys. G **38**, 053001 (2011).

[16] A. V. Anisovich, R. Beck, V. Burkert, E. Klempt, M. E. McCracken, V. A. Nikonov, A. V. Sarantsev, R. A. Schumacher, and U. Thoma, Energy-independent PWA of the reaction $\gamma p \to K^+\Lambda$, Eur. Phys. J. A **50**, 129 (2014).

[17] W. T. Chiang and F. Tabakin, Completeness rules for spin observables in pseudoscalar meson photoproduction, Phys. Rev. C **55**, 2054 (1997).

[18] R. L. Workman, L. Tiator, Y. Wunderlich, M. Döring, and H. Haberzettl, Amplitude reconstruction from complete photoproduction experiments and truncated partial-wave expansions, Phys. Rev. C **95**, 015206 (2017).

[19] R. L. Workman, M. W. Paris, W. J. Briscoe, L. Tiator, S. Schumann, M. Ostrick, and S. S. Kamalov, Model dependence of single-energy fits to pion photoproduction data, Eur. Phys. J. A **47**, 143 (2011).

[20] A. V. Anisovich, R. Beck, M. Döring, M. Gottschall, J. Hartmann, V. Kashevarov, E. Klempt, U. G. Meißner, V. Nikonov, M. Ostrick *et al.*, The impact of new polarization data from Bonn, Mainz and Jefferson Laboratory on $\gamma p \to \pi N$ multipoles, Eur. Phys. J. A **52**, 284 (2016).

[21] L. Tiator, R. L. Workman, Y. Wunderlich, and H. Haberzettl, Amplitude reconstruction from complete electroproduction experiments and truncated partial-wave expansions, Phys. Rev. C **96**, 025210 (2017).

[22] R. Koniuk and N. Isgur, Where have all the resonances gone? An analysis of baryon couplings in a quark model with chromodynamics, Phys. Rev. Lett. **44**, 845 (1980).

[23] E. Santopinto and J. Ferretti, Strange and nonstrange baryon spectra in the relativistic interacting quark-diquark model with a Gürsey and Radicati-inspired exchange interaction, Phys. Rev. C **92**, 025202 (2015).

[24] R. G. Edwards, N. Mathur, D. G. Richards, and S. J. Wallace (Hadron Spectrum Collaboration), Flavor structure of the excited baryon spectra from lattice QCD, Phys. Rev. D **87**, 054506 (2013).

[25] A. B. Migdal, The theory of nuclear reactions with production of slow particles, Zh. Eksp. Teor. Fiz. **28**, 3 (1955) [Sov. Phys. JETP **1**, 2 (1955)].

[26] K. M. Watson, The effect of final state interactions on reaction cross-sections, Phys. Rev. **88**, 1163 (1952).

[27] W. J. Briscoe, A. E. Kudryavtsev, I. I. Strakovsky, V. E. Tarasov, and R. L. Workman, On the photoproduction reactions $\gamma d \to \pi NN$, Eur. Phys. J. A **58**, 23 (2022).

[28] See, for example, B. H. Bransdon and R. G. Moorhouse, *The Pion-Nucleon System* (Princeton University Press, Princeton, NJ, 1973).

[29] C. Mullen *et al.* (A2 Collaboration at MAMI), Single π^0 production off neutrons bound in deuteron with linearly polarized photons, Eur. Phys. J. A **57**, 205 (2021); D. Glazier (private communication).

[30] R. A. Arndt, R. L. Workman, Z. Li, and L. D. Roper, Partial wave analysis of pion photoproduction, Phys. Rev. C **42**, 1853 (1990).

[31] R. A. Arndt, R. L. Workman, Z. Li, and L. D. Roper, Pion photoproduction resonance couplings in the second resonance region, Phys. Rev. C **42**, 1864 (1990).

[32] The SAID analyses are available through the GWU website http://gwdac.phys.gwu.edu/; W. J. Briscoe, M. Döring, H. Haberzettl, I. I. Strakovsky, and R. L. Workman, Institute of Nuclear Studies of The George Washington University Database.

[33] W. Chen, H. Gao, W. J. Briscoe, D. Dutta, A. E. Kudryavtsev, M. Mirazita, M. W. Paris, P. Rossi, S. Stepanyan, I. I. Strakovsky, V. E. Tarasov, and R. L. Workman, Amplitude analysis of $\gamma n \to \pi^- p$ data above 1 GeV, Phys. Rev. C **86**, 015206 (2012); W. Chen, T. Mibe, D. Dutta, H. Gao, J. M. Laget, M. Mirazita, P. Rossi, S. Stepanyan, I. I. Strakovsky, M. J. Amaryan *et al.*, A measurement of the differential cross section for the reaction $\gamma n \to \pi^- p$ from deuterium, Phys. Rev. Lett. **103**, 012301 (2009); W. Chen (private communication).

[34] M. Dugger *et al.* (CLAS Collaboration), Beam asymmetry Σ for π^+ and π^0 photoproduction on the proton for photon energies from 1.102 to 1.862 GeV, Phys. Rev. C **88**, 065203 (2013); M. Dugger (private communication).

[35] P. T. Mattione *et al.* (CLAS Collaboration), Differential cross section measurements for $\gamma n \to \pi^- p$ above the first nucleon resonance region, Phys. Rev. C **96**, 035204 (2017); P. T. Mattione (private communication).

[36] D. Ho *et al.* (CLAS Collaboration), Beam-target helicity asymmetry for $\vec{\gamma} \vec{n} \to \pi^- p$ in the N^* resonance region, Phys. Rev. Lett. **118**, 242002 (2017); F. Klein (private communication).

[37] W. J. Briscoe *et al.* (A2 Collaboration at MAMI), Cross section for $\gamma n \to \pi^0 n$ at the Mainz A2 experiment, Phys. Rev. C **100**, 065205 (2019); M. Martemianov (private communication).

[38] A. Švarc, M. Hadžimehmedović, H. Osmanović, J. Stahov, L. Tiator, and R. L. Workman, Pole positions and residues from pion photoproduction using the Laurent-Pietarinen expansion method, Phys. Rev. C **89**, 065208 (2014).

[39] D. Hornidge *et al.* (A2 and CB-TAPS Collaborations), Accurate test of chiral dynamics in the $\vec{\gamma} p \to \pi^0 p$ reaction, Phys. Rev. Lett. **111**, 062004 (2013); S. Prakhov (private communication).

[40] P. Adlarson *et al.* (A2 Collaboration at MAMI), Measurement of π^0 photoproduction on the proton at MAMI C, Phys. Rev. C **92**, 024617 (2015); S. Prakhov (private communication).

[41] V. Crede *et al.* (CBELSA/TAPS Collaboration), Photoproduction of neutral pions off protons, Phys. Rev. C **84**, 055203 (2011); V. Crede (private communication).

[42] M. C. Kunkel *et al.* (CLAS Collaboration), Exclusive photoproduction of π^0 up to large values of Mandelstam variables s, t and u with CLAS, Phys. Rev. C **98**, 015207 (2018); M. Kunkel (private communication).

[43] N. Muramatsu *et al.* (LEPS2 and BGOegg Collaborations), Measurement of neutral pion photoproduction off the proton with the large acceptance electromagnetic calorimeter BGOegg, Phys. Rev. C **100**, 055202 (2019); N. Muramatsu (private communication).

[44] S. Gardner *et al.* (A2 Collaboration at MAMI), Photon asymmetry measurements of $\vec{\gamma} p \to \pi^0 p$ for $E_\gamma = 320\text{-}650$ MeV, Eur. Phys. J. A **52**, 333 (2016); S. Gardner (private communication).

[45] J. Hartmann *et al.* (CBELSA/TAPS Collaboration), The polarization observables $\mathbb{T}$, $\mathbb{P}$, and $\mathbb{H}$ and their impact on $\gamma p \to p\pi^0$ multipoles, Phys. Lett. B **748**, 212 (2015); R. Beck (private communication).

[46] W. Luo *et al.* (GEp-III and GEp2gamma Collaborations), Polarization components in π^0 photoproduction at photon energies up to 5.6 GeV, Phys. Rev. Lett. **108**, 222004 (2012); W. Luo (private communication).

[47] S. Schumann *et al.* (A2 Collaboration at MAMI), Threshold π^0 photoproduction on transverse polarised protons at MAMI, Phys. Lett. B **750**, 252 (2015); S. Schumann (private communication).

[48] J. R. M. Annand *et al.* (A2 Collaboration at MAMI), $\mathbb{T}$ and $\mathbb{F}$ asymmetries in π^0 photoproduction on the proton, Phys. Rev. C **93**, 055209 (2016); V. Kashevarov (private communication).

[49] M. Gottschall *et al.* (CBELSA/TAPS Collaboration), First measurement of the helicity asymmetry for $\gamma p \to p\pi^0$ in the resonance region, Phys. Rev. Lett. **112**, 012003 (2014); R. Beck (private communication).

[50] N. Zachariou *et al.* (CLAS Collaboration), Double polarisation observable $\mathbb{G}$ for single pion photoproduction from the proton, Phys. Lett. B **817**, 136304 (2021); N. Zachariou (private communication).

[51] A. Thiel, A. V. Anisovich, D. Bayadilov, B. Bantes, R. Beck, Y. Beloglazov, M. Bichow, S. Bose, K. T. Brinkmann, T.

Challand *et al.*, Well-established nucleon resonances revisited by double-polarization measurements, Phys. Rev. Lett. **109**, 102001 (2012); A. Thiel (private communication).

[52] M. H. Sikora, D. P. Watts, D. I. Glazier, P. Aguar-Bartolome, L. K. Akasoy, J. R. M. Annand, H. J. Arends, K. Bantawa, R. Beck, V. S. Bekrenev *et al.*, Measurement of the $^1H(\vec{\gamma}, \vec{p})\pi^0$ reaction using a novel nucleon spin polarimeter, Phys. Rev. Lett. **112**, 022501 (2014); M. H. Sikora (private communication).

[53] S. Strauch *et al.* (CLAS Collaboration), First measurement of the polarization observable $\mathbb{E}$ in the $\vec{p}(\vec{\gamma}, \pi^+)n$ reaction up to 2.25 GeV, Phys. Lett. B **750**, 53 (2015); S. Strauch (private communication).

[54] W. J. Briscoe, A. E. Kudryavtsev, I. I. Strakovsky, V. E. Tarasov, and R. L. Workman, Threshold π^- photoproduction on the neutron, Eur. Phys. J. A **56**, 218 (2020); B. Strandberg, K. G. Fissum, J. R. M. Annand, W. J. Briscoe, J. Brudvik, F. Cividini, L. Clark, E. J. Downie, K. England, G. Feldman *et al.*, Near-threshold π^- photoproduction on the deuteron, Phys. Rev. C **101**, 035207 (2020).

[55] W. J. Briscoe, A. E. Kudryavtsev, P. Pedroni, I. I. Strakovsky, V. E. Tarasov, and R. L. Workman, Evaluation of the $\gamma n \to \pi^- p$ differential cross sections in the Delta-isobar region, Phys. Rev. C **86**, 065207 (2012); J. Ahrens, S. Altieri, J. R. M. Annand, H. J. Arends, R. Beck, M. A. Blackston, C. Bradtke, A. Braghieri, N. d'Hose, H. Dutz *et al.*, Helicity dependence of the $\gamma d \to \pi NN$ reactions in the Delta-resonance region, Eur. Phys. J. A **44**, 189 (2010); M. M. Fabregate, PhD thesis, Johannes Gutenberg University of Mainz (2007); P. Pedroni (private communication).

[56] D. Sokhan *et al.* (CLAS Collaboration), A new measurement of beam asymmetry in pion photoproduction from the neutron using CLAS, Int. J. Mod. Phys. A **24**, 497 (2009); D. Sokhan, Beam asymmetry measurement from pion photoproduction on the neutron, PhD thesis, University of Edinburgh (2009); (private communication).

[57] M. Dieterle *et al.* (A2 Collaboration at MAMI), Photoproduction of π^0 mesons off protons and neutrons in the second and third nucleon resonance region, Phys. Rev. C **97**, 065205 (2018); M. Dieterle (private communication).

[58] M. Dieterle, L. Witthauer, F. Cividini, S. Abt, P. Achenbach, P. Adlarson, F. Afzal, Z. Ahmed, C. S. Akondi, J. R. M. Annand *et al.*, First measurement of the polarization observable $\mathbb{E}$ and helicity-dependent cross sections in single π^0 photoproduction from quasi-free nucleons, Phys. Lett. B **770**, 523 (2017); M. Dieterle (private communication).

[59] D. G. Ireland, E. Pasyuk, and I. Strakovsky, Photoproduction reactions and non-strange baryon spectroscopy, Prog. Part. Nucl. Phys. **111**, 103752 (2020).

[60] I. Strakovsky, S. Širca, W. J. Briscoe, A. Deur, A. Schmidt, and R. L. Workman, Single-pion contribution to the Gerasimov-Drell-Hearn sum rule and related integrals, Phys. Rev. C **105**, 045202 (2022).

[61] M. Dugger, B. G. Ritchie, J. P. Ball, P. Collins, E. Pasyuk, R. A. Arndt, W. J. Briscoe, I. I. Strakovsky, R. L. Workman, G. S. Adams *et al.*, π^0 photoproduction on the proton for photon energies from 0.675 to 2.875-GeV, Phys. Rev. C **76**, 025211 (2007).

[62] K. Wijesooriya, A. Afanasev, M. Amarian, K. Aniol, S. Becher, K. Benslama, L. Bimbot, P. Bosted, E. J. Brash, J. Calarco *et al.*, Polarization measurements in neutral pion photoproduction, Phys. Rev. C **66**, 034614 (2002).

[63] M. Dugger *et al.* (CLAS Collaboration), π^+ photoproduction on the proton for photon energies from 0.725 to 2.875-GeV, Phys. Rev. C **79**, 065206 (2009).

[64] R. Di Salvo, A. Fantini, G. Mandaglio, F. Mammoliti, O. Bartalini, V. Bellini, J. P. Bocquet, L. Casano, A. D'Angelo, J. P. Didelez *et al.*, Measurement of Sigma beam asymmetry in π^0 photoproduction off the neutron in the second and third resonances region, Eur. Phys. J. A **42**, 151 (2009).

[65] R. A. Arndt, J. M. Ford, and L. D. Roper, Pion-nucleon partial wave analysis to 1100-MeV, Phys. Rev. D **32**, 1085 (1985).

[66] P. J. Bussey, C. Raine, J. G. Rutherglen, P. S. L. Booth, L. J. Carroll, G. R. Court, P. R. Daniel, A. W. Edwards, R. Gamet and C. J. Hardwick *et al.*, Polarization parameters in neutral pion photoproduction, Nucl. Phys. B **154**, 492 (1979).

[67] E. Gutz *et al.* (CBELSA/TAPS Collaboration), High statistics study of the reaction $\gamma p \to p \pi^0 \eta$, Eur. Phys. J. A **50**, 74 (2014); The Bonn–Gatchina analyses (BnGa19) are available through the Bonn website: http://pwa.hiskp.uni-bonn.de/.

[68] F. V. Adamian, P. I. Galumian, V. O. Grabsky, G. G. Akopian, V. K. Oktanian, G. V. Karapetian, V. V. Karapetian, and G. A. Vartapetian, Single π^- meson photoproduction on neutrons by linearly polarized photons in the third and fourth resonance region, J. Phys. G **15**, 1797 (1989).

[69] C. R. Clinesmith, π^0 photoproduction from the deuteron at forward angles in the energy range from 900-MeV to 1400-MeV, RX-184; PhD thesis, California Institute of Technology, 1967.

[70] R. L. Workman, L. Tiator, and A. Sarantsev, Baryon photodecay amplitudes at the pole, Phys. Rev. C **87**, 068201 (2013).

[71] R. L. Workman, R. A. Arndt, W. J. Briscoe, M. W. Paris, and I. I. Strakovsky, Parameterization dependence of T matrix poles and eigenphases from a fit to πN elastic scattering data, Phys. Rev. C **86**, 035202 (2012).

[72] V. Sokhoyan *et al.* (CBELSA/TAPS Collaboration), High-statistics study of the reaction $\gamma p \to p \, 2\pi^0$, Eur. Phys. J. A **51**, 95 (2015); V. Sokhoyan, *ibid.* **51**, 187 (2015).

[73] A. V. Anisovich, V. Burkert, N. Compton, K. Hicks, F. J. Klein, E. Klempt, V. A. Nikonov, A. M. Sandorfi, A. V. Sarantsev, and U. Thoma, Neutron helicity amplitudes, Phys. Rev. C **96**, 055202 (2017).

[74] A. V. Anisovich, R. Beck, E. Klempt, V. A. Nikonov, A. V. Sarantsev, and U. Thoma, Properties of baryon resonances from a multichannel partial wave analysis, Eur. Phys. J. A **48**, 15 (2012).

[75] D. Rönchen, M. Döring, U. G. Meißner, and C. W. Shen, Light baryon resonances from a coupled-channel study including **KΣ** photoproduction, Eur. Phys. J. A **58**, 229 (2022).

[76] R. G. Moorhouse, Photoproduction of N^* resonances in the quark model, Phys. Rev. Lett. **16**, 772 (1966).